The Impacts of Wildfires on Ozone Production and Boundary Layer Dynamics in California's Central Valley

Keming Pan and Ian C. Faloona

Department of Land, Air, & Water Resources and the Air Quality Research Center, University of California, Davis, 95616, USA

Correspondence to: Keming Pan (kmpan@ucdavis.edu)

Abstract. We investigate the role of wildfire smoke on ozone photochemical production ($P(O_3)$) and atmospheric boundary layer (ABL) dynamics in California's Central Valley during June-September, 2016-2020. Wildfire events are identified by the Hazard Mapping System (HMS) and the Hybrid Single Particle Lagrangian Integrated Trajectory Model (HYSPLIT). Air quality and meteorological data are analyzed from 10 monitoring sites operated by the California Air Resources Board (CARB) across the Central Valley. On average, wildfires were found to influence air quality in the Central Valley on about 20% of the total summer days of the study. During wildfire influenced periods, maximum daily 8h averaged (MDA8) O_3 was enhanced by about 5.5 ppb or 10% of the median MDA8 (once corrected for the slightly warmer temperatures) over the entire valley. Overall, nearly half of the total exceedances of the National Ambient Air Quality Standards (NAAQS) where MDA8 O_3 > 70 ppb, occur under the influence of wildfires, and approximately 10% of those were in exceedance by 5 ppb or less indicating circumstances that would have been in compliance with the NAAQS were it not for wildfire emissions. The photochemical ozone production rate calculated from the modified Leighton relationship was also found to be higher by ~~26~~50% on average compared to non-fire periods despite the average diminution of $j(NO_2)$ by ~7% due to the shading effect of the wildfire smoke plumes. ~~Furthermore, the in-situ ozone production rates are found to be elevated due to enhancement of both peroxy radicals and NO in near equal measure.~~ Surface heat flux measurements from two AmeriFlux sites in the Northern San Joaquin Valley show midday surface buoyancy fluxes decrease by 30% on average when influenced by wildfire smoke. Similarly, afternoon peak ABL heights measured from a radio acoustic sounding system (RASS) located in Visalia in the Southern San Joaquin Valley were found to decrease on average by 80 m (~15%) with a concomitant reduction of downwelling shortwave radiation of 54 Wm^{-2}, consistent with past observations of the dependence of boundary layer heights on insolation.

Keywords   Boundary Layer Dynamics · California's Central Valley · Ozone Photochemistry · Wildfire · NAAQS

1   Introduction

Ozone (O_3) pollution poses a threat to public health and the environment. Excessive O_3 exposure is known to damage the tissues of the respiratory tract causing a variety of symptoms such as chest pain, coughing, emphysema, asthma, and leading to the need for increased medical care (Rombout et al., 1986). Apart from that, O_3 also causes substantial damage to crops,

forests, and native plants (Ainsworth, 2017). Tropospheric O_3 is produced from the chemical reaction of nitrogen oxides (NO_x=NO+NO_2) and volatile organic compounds (VOCs) in the presence of sunlight. Figure 1 shows the schematic representation of the photochemical formation of O_3 in the presence of NO_x and VOCs (Jenkin and Hayman, 1999). Equation (R1)-(R5) are the major reactions in this process where R represents a generalized organic moiety from the initial VOC.
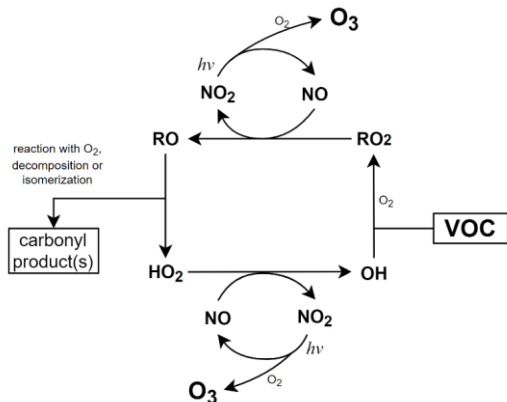

Figure 1: Schematic representation of the photochemical formation of O_3 in the presence of NO_x and VOCs (Jenkin & Hayman, 1999)).

$$NO_2 + h\upsilon \rightarrow NO + O(^3P) \tag{R1}$$
$$O_3 + NO \rightarrow NO_2 + O_2 \tag{R2}$$
$$HO_2 + NO \rightarrow NO_2 + OH \tag{R3}$$
$$RO_2 + NO \rightarrow NO_2 + RO \tag{R4}$$
$$O_2 + O(^3P) + M \rightarrow O_3 + M \tag{R5}$$

Wildfires emit large amounts of primary pollutants, like black carbon (BC), carbon monoxide (CO), NO_x and VOCs. Studies of boreal fire emissions show that the NO_x concentrations can be doubled , and BC increased by 10 times when influenced by wildfires, even 1-2 weeks downwind in the middle of the Atlantic Ocean (Val Martín et al., 2006). The wildfire impacts on O_3 production is a complex process involving various factors, such as fire precursor emissions, altered photochemical reactions, the effect on radiation by aerosols from the smoke plume, and local and downwind meteorological patterns (Jaffe and Wigder et al., 2012). Previous studies indicate that both NO_x and VOCs emissions from wildfires influence the O_3 budgets downwind, with enhancements ranging from 5 to 20 ppb (Baylon et al., 2015; Buysse et al., 2019; Jaffe and Wigder et al., 2012; McClure et al., 2018; Ninneman et al., 2021; Selimovic et al., 2020; Val Martín et al., 2006). When wildfire smoke reaches urban regions, the NO_x, and VOCs in the smoke is believed to enhance O_3 production (Akagi et al., 2013; Singh et al., 2012) and exacerbate the already problematic O_3 pollution levels in many urban areas. Brey and Fischer (2016) found that the mean O_3 abundance measured on smoke-impacted days is higher than smoke-free days and the magnitude varies by location with a range of 3 to 36 ppbv. Furthermore, they found that the smoke-impacted O_3 mixing ratios are most elevated in locations with the highest emissions of NO_x.

However, the O_3 response can vary from significant to small enhancements and even depletion during different wildfire events (Val Martín et al., 2006). Buysse et al. (2019) and McClure & Jaffe (2018) also report that maximum daily 8h averaged (MDA8) O_3 tends to decrease during heavy smoke influenced period when $PM_{2.5}$ (particulate matter with diameters that are smaller than 2.5 µm) exceeds 70 µg/m^3. The reasons for this are not fully understood but may be explained by some of the following conjectures in the literature. Alvarado et al. (2010) found that on average 40% of the NO_x was converted to peroxyacetyl nitrate (PAN) within 1-2 hours after emission, thus limiting NO_x availability and in-situ O_3 production. The potential loss of O_3 due to reaction with organic carbon could decrease O_3 concentrations in wildfire plumes. For example, de Gouw and Lovejoy (1998) found that heterogeneous reaction between O_3 and organic aerosol can be an important loss for tropospheric O_3, particularly if the aerosols contain unsaturated organic material. Fischer et al. (2010) found O_3 enhancements of about 20 ppb at a site downwind of a wildfire and estimated that about 8 ppb could be attributed to the decomposition of PAN during adiabatic warming during subsidence. Moreover, Buysee et al. (2019) found lower NO/NO_2 ratios when sites are influenced by wildfire smoke and suggested several potential reasons including elevated atmospheric oxidants (O_3, RO_2 and HO_2), higher temperature, lower rates of NO_2 photolysis due to shading, and increased interference in the NO_2 measurements by other nitrogen species present in the wildfire smoke. A recent modeling study investigating a 2013 California wildfire showed that the simulation of near-fire smoke plume transport appears to perform well compared to satellite and aircraft measurements (Baker et al., 2018). While the photolysis rates in that study were also found to be well-characterized by the model, the predicted O_3, on the other hand, did not compare well with either surface site nor aircraft measurements: O_3 was overestimated by the model both aloft and at the surface during periods impacted by wildfires anywhere from 5 to over 50 ppb.

As alluded to already, the vast amounts of absorbing aerosols like brown and black carbon emitted from biomass burning could also influence the amount of radiation that reaches the surface. Airborne studies using aerosol and radiation measurements indicate that a layer of high aerosol loading lying below a temperature inversion could drastically reduce the downwelling solar and UV irradiance, including the surface $j(NO_2)$ (Wendisch et al., 1996). Baylon et al. (2018) conducted an investigation of wildfire impacts on O_3 production at a high elevation site located on Mt. Bachelor in Oregon, and report $j(NO_2)$ decreasing by 14 to 21% at high solar zenith angles when biomass burning plumes were detected, but slightly increasing (0.2~1.8%) at local noon. Furthermore, meteorological factors that may be correlated with wildfires and the conditions that lead to their proliferation such as temperature and humidity, could potentially affect the reactions associated with O_3 production (Lin et al., 2017; Zhang et al., 2014). One study of the temperature dependence of O_3 production in the San Joaquin Valley (SJV) (Pusede et al., 2014), for instance, found that the reactivity of total VOCs with OH (s^{-1}) and the HO_x production rate (PHO_x ppts^{-1}) both increased exponentially with temperature, leading to higher midday O_3 concentrations by 1.5 -2.0 ppb/K. Steiner et al. (2010) also reported similar temperature dependencies on maximum 1hr ozone levels while underscoring their decreasing trend over the 25 years of their study, assumed to be a consequence of reducing NO_x and VOC emissions across the state.

In the United States, the current National Ambient Air Quality Standards (NAAQS) for ozone is an MDA8 value equal to or exceeding 70 ppb. According to the California Air Resource Board (CARB), O_3 concentrations frequently exceed existing health-protective standard in metropolitan areas of California during summertime. In addition, the southern part of California's Central Valley (CV), the San Joaquin Valley (SJV), is still one of the two extreme O_3 nonattainment areas

remaining in the U.S. (U.S. EPA Green Book, www.epa.gov/green-book). With the projection of an increasing likelihood of large wildfires in the future across the western U.S. (Brey et al., ~~2020~~2021; Stavros et al., 2014), it is important to understand

95 how O_3 production will change subject to the rising influence of wildfire events in the CV, and it will also be useful for the regulator to predict air quality degradation in the case of wildfire events.

In addition to the impacts of wildfires on air quality, Pahlow et al. (2005) present a proposed phenomenon that the shading effect of wildfire smoke can reduce the solar heating of the ground and lead to a shallower ABL, but the data evinced was only for three consecutive days on the US east coast. That study raises the question of whether the attenuation of ABL

100 height due to wildfire shading is a general phenomenon and might it be supported by long-term observations. The strong correlation between downwelling surface solar radiation and ABL height has been described by previous studies. Pal and Haeffelin (2015) implemented a 5-year observational study of ABL height and surface fluxes near Paris in which they found the strongest determinant (r=0.92) of daily maximum ABL height was maximum downwelling shortwave radiation at the surface (SSWD), more so even than the surface heat flux (r=0.5). The strong correlation between SSWD and afternoon ABL

105 height was also verified by Trousdell et al. (2016) in the SJV with a similar dependence of $1.5 – 1.7$ m per Wm^{-2}. The lowest portion of the free troposphere (FT) in the SJV has a complex structure with a 'buffer layer' residing between ABL and FT, which is a layer of relatively stagnant air at altitudes between 500m to 2500m resulting from the onshore wind that impinges on the Southern Sierra Nevada mountains on the east side of the SJV (Faloona et al., 2020). This 'buffer layer' accumulates the pollutants from the ABL by anabatic sidewall venting during the daytime but continuously returns some of the air via

110 midday entrainment, with turbulence within the ABL being the key factor that controls the entrainment process. If the shading effect of wildfire smoke can considerably influence the ABL dynamics or ABL height, then it will be important to quantify the amount of ABL height attenuation that results from wildfire smoke and elucidate the impacts on the ventilation of pollutants in the SJV because entrainment has a direct impact on surface level concentrations of most pollutants (Trousdell et al., 2019).

115 In this paper, we use data from 10 CARB monitoring sites in the CV to quantify the impacts of wildfire smoke during summer (Jun-Sep) from 2016 to 2020. Then we use measured O_3, NO and NO_2 (corrected approximately for known interferences) in a modified Leighton relationship (Volz-Thomas et al., 2003) to estimate changes to the O_3 production rate $P(O_3)$, accounting for the observed shading effect of the wildfire smoke on $j(NO_2)$, as well as variations in ambient O_3, and k_{O_3+NO} (rate constant in Eq. (R2)) due to temperature variations. In this way we are able to identify the specific impacts of

120 wildfire emissions on regional ozone chemistry whereas past studies have tended to leave these impacts mingled together. We also present the enhancement ratios (ERs) for O_3/T, $PM_{2.5}$/CO, and O_3 production efficiency (OPE) during the wildfire influenced periods in the CV. Then, we discuss the influences of wildfire smoke on surface buoyancy and heat fluxes ($\overline{w'\theta_v'}$, Q_H, and Q_E) measured by two AmeriFlux monitoring sites located in the northern part of the SJV. We also use a radio acoustic sounding system (RASS) located near Visalia to study wildfire impacts on temperature profiles and ABL heights.

125 Our study aims at using long-term observation data to quantify the differences of O_3 concentrations and production rates during the wildfire influenced periods in the CV and providing insights into the alteration of ABL dynamics that occurs in the presence of wildfire smoke.

## 2 Data and Methods

2.1 Measurements

Measurements of hourly $PM_{2.5}$, O_3, nitric oxide (NO), nitrogen dioxide (NO_2), and CO are taken from 10 CARB monitoring sites in the CV. Meteorological data, such as temperature, dew point, and pressure are supplemented when needed from airports nearest each air pollution monitoring site. Figure 2 shows a map (© Google Earth 2020) for the locations of CARB sites as well as the RASS site and AmeriFlux sites used in our study. The locations and other detailed information about the sites can be found in Table 1. All the air pollution and meteorological data were download via the CARB website (https://www.arb.ca.gov/aqmis2/aqmis2.php), except for the data on reactive nitrogen compounds (NO_y), which was downloaded via AirNow-Tech (http://www.airnowtech.org). The CARB gather air quality data for the State of California, ensures the quality of this data, designs, and implements air models, and sets ambient air quality standards for the state. The standard operating procedures for ambient air monitoring can be found on the CARB website (https://ww2.arb.ca.gov/resources/documents/standard-operating-procedures-ambient-air-monitoring). The hourly-averaged data start at the beginning of the reported time. Singular missing hourly measurements are replaced by the average of the hour before and after, otherwise missing data are disregarded. We found that 1.9% of the 24-hr $PM_{2.5}$ and 1.5% of the MDA8 O_3 data are not available due to missing or erroneous values. We use temperature and relative humidity data from the CARB monitoring sites if they are available, otherwise we use measurements from meteorological sites at the nearest airport (Downloaded via AirNow-Tech, provided by Meteorological Assimilation Data Ingest system https://madis-data.ncep.noaa.gov (i.e., MADIS)). Since relative humidity is a function that strongly depends on temperature, we also calculate specific humidity (q) from pressure measurements at the airport and the Clausius-Clapeyron relationship to eliminate the direct dependence on temperature. Because approximately 80% of O_3 exceedance days in the SJV typically occur between June 1 and September 30 (Trousdell et al., 2019), we focus on this period for each year (2016-2020). We calculate 24-hr $PM_{2.5}$ and MDA8 O_3 as daily metrics, and the average of other pollutant concentrations are from 10:00 and 15:00 Pacific Standard Time (PST) as daytime averages that are most relevant to peak ozone levels.

The conventional measurement of NO_2 entails the catalytic conversion of NO_2 to NO on a heated molybdenum (Mo) surface and subsequently measured by chemiluminescence after reaction with O_3. The drawback of this method is that other oxidized nitrogen compounds such as PAN and HNO_3 can also be converted to NO, thus the molybdenum conversion method is known to cause overestimation of NO_2. Steinbacher et al. (2007) proposed a correction method for overestimated NO_2 measurements based on their long-term observations in rural Switzerland via Eq. (6):

$$\Delta NO_2 = a \cdot (NO_2)_m + b \cdot O_3 + c \cdot f(month) + d \cdot f(day) + e + \varepsilon \tag{6}$$

where ΔNO_2 is the amount of overestimation for NO_2, $(NO_2)_m$ is the measured NO_2 concentration, O_3 is measured ozone concentration. a, b, c, d, e, and $f(month)$ are constants, and $f(day)$ is binary predictor distinguishing day time and night time (1 or 0), and ε is a residual noise term that we ignored in our study. Details about those constants can be found in Table C1. ~~All the NO₂ measurements~~ The NO_2 at the Sacramento site is measured using a photolytic converter, which should not be affected by the interference from other oxidized nitrogen compounds to a large degree. All the NO_2 measurements except for those from the Sacramento site in this study are corrected according to Eq. (6), with the resultant NO_2 decreasing on average by about 1.~~5~~3 ppb (~30%) after the correction. This is not meant to perfectly eliminate all of the potential interferences in this measurement but is intended to eliminate the bulk of the interferences that are known to exist with this analytical technique.

5

165   A similar analysis of the interference in the heated Mo technique, relative to a spectral NO_2 measurement, was reported by Dunlea et al. (2007) in Mexico City, a very different environment, in which they found the long-term average to be ~22% in excess. ~~While~~Furthermore, the suburban sites reported in Xu et al. (2013) showed corrections also in-line with what we ~~know there are likely different mixtures~~used in this study, which is midday summertime values of ~~interferences in a tropical megacity, a central European rural environment~~25%-40%. In general, it is found that the Mo-chemiluminescence interference

170   is proportionally smallest in urban regions, moderate in suburban regions, and ~~the~~ highest in remote regions. We believe that the Central Valley of California is somewhere between urban and suburban/rural in its air quality and therefore the Steinbacher et al. (2007) correction we use from their urban/rural ~~mix of the CV, we apply this correction~~ site is reasonably appropriate in order to remove the first-order complications of this widespread chemiluminescence measurement. In Section 3.2 we investigate the uncertainty that introduced to our estimation of the $P(O_3)$ due to errors of measurements in NO_2.
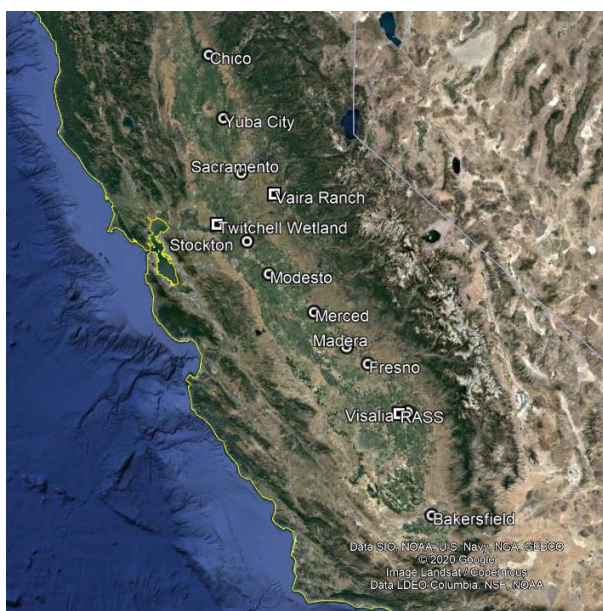
175   **Figure 2: A map of the locations of CARB sites (circles), RASS site and AmeriFlux sites (squares) used in this study (© Google Earth 2020).**

Table 1: The locations of measurement sites and detailed information.

Site Name	Site Location (°N, °~~E~~W)	Agency	Measurements
Chico-East	39.76, –121.84	CARB	O_3, $PM_{2.5}$, CO, NO, NO_2, T, RH
MADIS-KCIC	39.80, –121.85	MADIS	U, RH (2016)

Formatted Table

6

Yuba City	39.14, –121.62	CARB	O_3, $PM_{2.5}$, NO, NO_2, T, RH
MADIS-KMYV	39.10, –121.57	MADIS	U, P, RH (2016-2017)
Sutter Buttes	39.21, –121.82	CARB	CO (2017-2019)
Arden Arcade - Del Paso Manor	38.61, –121.37	Sacramento Metro. AQMD	O_3, $PM_{2.5}$, CO (2016-2019), NO, NO_2, T, RH, U, P
Stockton - Hazelton Street	37.95, –121.27	CARB	O_3, $PM_{2.5}$, CO, NO, NO_2, T, RH
MADIS-KSCK	37.90, –121.25	MADIS	U, P, RH (2016)
Modesto - 14th Street	37.64, –120.99	CARB	O_3, $PM_{2.5}$, CO, T, RH
MADIS-KMOD	37.63, –120.95	MADIS	U, P, RH (2016)
Merced - S. Coffee Ave	37.28, –120.43	CARB	O_3, $PM_{2.5}$, NO, NO_2, T, RH, U
Madera-City	36.95, –120.03	San Joaquin Valley Unified APCD	P, $PM_{2.5}$
Madera - Pump Yard	36.87, –120.01	San Joaquin Valley Unified APCD	O_3, CO, NO, NO_2, T, RH, U
Fresno - Garland	36.79, –119.77	CARB	O_3, $PM_{2.5}$, CO, NO, NO_2, T, RH
MADIS-KFAT	36.77, –119.72	MADIS	U, P, RH (2016)
Visalia - N. Church Street	36.33, –119.29	CARB	O_3, $PM_{2.5}$, NO, NO_2, T, RH
MADIS-KVIS	36.32, –119.40	MADIS	U, P, RH (2016)
Bakersfield - California Ave	35.36, –119.06	CARB	$PM_{2.5}$
Bakersfield-Muni	35.33, –119.00	San Joaquin Valley Unified APCD	O_3, CO, NO, NO_2, T, RH, U, P

Formatted Table

2.2 Wildfire identification

180   We use the NOAA Hazard Mapping System (HMS) Fire and Smoke Product and the Hybrid Single Particle Lagrangian Integrated Trajectory (HYSPLIT) model accessed from AirNow-Tech (https://www.airnowtech.org/index.cfm) as an identification tool for wildfire events. The HMS is an interactive environmental satellite image display and graphical system that was developed by National Environmental Satellite, Data, and Information Service. The HMS is used by trained satellite analysts to generate a daily operational list of fire locations and outline areas of smoke (Brey et al., 2018). The analysts also

185   rely primarily on visible satellite images to confirm that the fire locations are actually producing smoke. Then these detected points of fire locations are used to initiate the HYSPLIT model by NOAA, which is a complete system for computing simple air parcel trajectories, as well as complex transport, dispersion, chemical transformation, and deposition simulations (Stein et al., 2015), to estimate the movement of smoke in the NWS (National Weather Service) smoke forecast (Rolph et al., 2009; Ruminski et al., 2006). The HMS creates a fresh map for North America daily around 7-8 a.m. Eastern time. For the

190   performance time of the HMS in the CV (4-5 a.m. PST), this may cause a situation wherein the site is not detected by HMS with overhead smoke early in the morning but could be covered by smoke the rest of the day. In addition, because the HMS system is a satellite-based product, it is observed from above, therefore it cannot differentiate surface wildfire plumes from lofted plumes and may also be limited by any cloud cover. These limitations may cause improper identification of wildfire events; therefore, we use additional methods to verify the presence of wildfire smoke at the surface level. Thus, we also use

195   the HYSPLIT model to analyze the back-trajectories of the air parcels starting at each target site and trace its origin at surface level and within the ABL. By using the HMS and HYSPLIT, the steps for wildfire identification are as follows. First, we use the HMS product to see if any sites are covered by smoke. The target sites that are covered by the HMS smoke are marked according to the category of the HMS product as thin, medium, and thick smoke coverage. Second, we use the HYSPLIT model to calculate 24-hour back-trajectories at 12:00 p.m. PST starting from the sites that are covered with the HMS wildfire

200   smoke areas. The HYSPLIT model is performed at altitudes of 100m, 600m and 1500m, respectively, with a resolution of 12km (NAM 12km), which will provide the transport pattern near the surface, the top of boundary layer and in the middle of the "buffer layer" (Faloona et al., 2020) or what is sometimes called the "stable core layer" (Leukauf et al., 2016) of a valley atmosphere. Given that the low-level flow in the CV has a well-characterized diurnal pattern during summertime (Zhong et al., 2004), we think that the HYSPLIT back-trajectory performed at 3 different levels are enough to represent the transport

205   pattern of the air flow near the surface during our periods of study. If the HMS shows overhead smoke coverage and one of the HYSPLIT back-trajectories originated from or passed by the area of fire spots detected by the HMS, we define the target site as influenced by wildfire smoke on that day. The purpose of our method involving both the HMS system and the HYSPLIT model is to identify cases that contain a significant impact of wildfire smoke at the surface level as accurately as possible. We believe that even if the fire plume is overhead and the back-trajectory ends above the ABL, strong daytime

210   subsidence and entrainment over the valley will likely bring the wildfire effluent into the ABL and affect surface concentrations of air pollutants. Moreover, we also need a baseline to provide the conditions (e.g., pollutant concentrations, ABL height) without the influences of wildfire smoke to use as a control sample. We use images from the true color reflectance of MODIS Aqua and Terra to identify the days that are without cloud coverage and immediately before and after the wildfire influenced periods as our baseline. In the following paragraphs, we will refer to those as the background or non-

215   fire days. In this way, we are able to identify the wildfire events at each site and then use the baseline from background days to compare with the cases when the wildfire smoke is present at surface level.

2.3 O_3 production

    The modified Leighton relationship is a method to determine the relative magnitude of the in-situ photochemical O_3 production rate by measuring the extent to which the O_3-NO_x cycle is away from the photostationary state. This method

220   represents the photochemical cycle of O_3, NO_x, HO_2 and RO_2 (Leighton, 1961). The chemical reactions entailed in this cycle are in Eq. (R1)-Eq. (R4), where $j(NO_2)$ is the photolysis rate in Eq. (R1), k_{O_3}, k_{HO_2} and k_{RO_2} are reaction rate coefficients for Eq. (R2), (R3) and (R4), respectively. The role of wildfire smoke will include the addition of NO_x and VOCs, which results in changing the concentration of HO_2 , RO_2, NO_x and their ensuing effects on O_3 production.

$$\frac{[NO]}{[NO_2]} = \frac{j(NO_2)}{k_{O_3}[O_3]+k_{HO_2}[HO_2]+k_{RO_2}[RO_2]} \tag{7}$$

225   The O_3 production rate is derived from the modified Leighton relationship presented in Eq. (7). Equation (R3) and (R4) determine the limiting rates for O_3 production, thus the production rate of NO_2 in Eq. (R3) and (R4) is the effective production rate for 'new' O_3 that does not belong to the instantaneous photostationary state cycle. This can be expressed as:

$$P(O_3) = [NO]\{k_{HO_2}[HO_2]+k_{RO_2}[RO_2]\} = j(NO_2)[NO_2] - k_{O_3}[O_3][NO] \tag{8}$$

where $[NO]$, $[NO_2]$ and $[O_3]$ are hourly averaged mixing ratio measured by CARB, and $k_{HO_2}[HO_2]+k_{RO_2}[RO_2]$ represent the

230   contributions of VOC (and CO) in O_3 production. The direct measurements of $j(NO_2)$ at ground level are not often available in field studies. Trebs et al. (2009) reported a relationship that can be used to estimate ground-level $j(NO_2)$ directly from the solar irradiance, which is measured as a standard parameter in most field measurements. In the absence of direct measurement of $j(NO_2)$, this method is more reliable than radiative transfer calculations with poorly known input parameters. We use surface solar radiation measurements from California Irrigation Management Information System (CIMIS,

235   https://cimis.water.ca.gov/WSNReportCriteria.aspx) to calculate the hourly $j(NO_2)$ by using a second-order polynomial function (A1) in Trebs et al. (2009) study. This approach is employed to account for the decreased photolysis rates during wildfire events due to the shading effect of the overhead smoke. Moreover, k_{O_3} is also adjusted to corresponding hourly-averaged temperature measured at each site to account for the changes of rate coefficients due to temperature change using Eq. (A2) (Lippmann et al., 1980).

240   ~~The concentration of HO_2 and RO_2 is estimated from Eq. (8) and we consider the sum of HO_2 and RO_2 as RO_x. The rate constants for Eq. (R5) and (R6) are within ~5% at 310 K (Brasseur et al., 1999), so we assume they are equal and solve for total RO_x, the results are presented as the effective first-order reaction rate $k[RO_x]$ (s^+). Although $HO_2 + RO_2$ tends to be overestimated by using this method (Griffin et al., 2007; Mannschreck et al., 2002; Volz-Thomas et al., 2003), we still consider it useful when comparing the relative differences between wildfire-influenced and background periods in order to~~

245   ~~investigate the impact of additional RO_x or VOC, distinct from changes in NO and $j(NO_2)$ on the overall in-situ photochemical O_3 production rates.~~

2.4 Boundary layer dynamics

We use surface eddy covariance flux data from two AmeriFlux sites located at Twitchell Wetland (Knox et al., 2018) (38.1074 N, 121.6469 W, -5m) and Vaira Ranch (Ma et al., 2021) (38.4133 N, 120.9507 W, 129m). The Twitchell site has a flux tower equipped to analyze energy, H_2O, CO_2, and CH_4 fluxes since May 2012, which is located at a 7.4-acre restored wetland on Twitchell Island. The wetland is almost completely covered by cattails and tules by the third growing season. Vaira Ranch site has been established at the lower foothills of the Sierra Nevada mountains on privately owned land since 2000; the site is classified as a grassland dominated by C3 annual grasses. The measurements at the two sites include surface sensible heat flux (Q_H), latent heat flux (Q_E), temperature, incoming shortwave radiation, and the mole fraction of water vapor. The time resolution is 30 minutes, and the measurements are available from 2016 to 2019. The surface buoyancy flux is calculated by Eq. (9), where $\bar{\theta}$, $\overline{w'\theta'}$ and $\overline{w'q'}$ are direct measurement from the site, and $\bar{q}$ is calculated from the measured mole fraction of water vapor.

$$\overline{w'\theta_v'} \cong \overline{w'\theta'}(1 + 0.61\bar{q}) + 0.61\bar{\theta}\,\overline{w'q'} \tag{9}$$

We use the same wildfire events identification results from section 2.2 to categorize wildfire days and background days, where Twitchell Island (30km northwest of Stockton) uses the results of Stockton and Vaira Ranch (50 km southeast of Sacramento) uses the result of Sacramento. Then, we calculate the averaged diurnal profile for $\overline{w'\theta_v'}$, Q_H, Q_E, and incoming shortwave radiation for wildfire-influenced and background days at each site.

Radio acoustic sounding systems (RASS) remotely measure the virtual temperature and wind profile up to about 2km, and their 1-hour time resolution has substantial advantages over radiosondes. We use the virtual temperature data measured by the RASS located near the Visalia Municipal Airport. Then, the virtual temperature is converted into virtual potential temperature by the hypsometric and Poisson's equations based on the surface measurements of temperature and pressure. The ABL height is estimated by the first range gate where the vertical virtual potential temperature gradient exceeds 10 K/km. Then, the estimated ABL heights are also sorted into wildfire influenced days and background days for comparison. A 5-year monthly averaged diurnal ABL height profile retrieved by this method during June to September, 2016-2020 is shown in Fig. B4. The magnitude and timing of the ABL heights correspond approximately to the diurnal ABL profiles in the SJV measured by Bianco et al. (2011) and Faloona et al. (2020).

3 Results and Discussion

3.1 Summary of wildfire events from 2016 to 2020

During the summer time (June to September) in the CV, wildfires are prone to happen amidst the mountains that surround the valley and spread upslope in general. The yearly acres burned by wildfire in California during the study ranges from 259,148 in 2019 to 1,823,153 in 2018 (National Interagency Coordination Center, https://www.nifc.gov/fireInfo/fireInfo_statistics.html). By September 2020, the 2020 fire season in California had become the most intense year of the 18-year long fire radiative power measurements collected by satellite (NOAA/NESDIS Hazard Mapping System, https://www.ospo.noaa.gov/Products/land/hms.html). The number of wildfire-influenced days at each site are presented in Table C2. Although the wildfire-influenced days vary from site to site, the average total number of the wildfire days are about 120 days out of 600 days (~20%) from our 5-year data analysis (2016-2020). The composite means of

the 500 hPa geopotential height fields are shown in Figure B5 indicating that the climatological coastal trough is more dominant during the background days, and the high-pressure bulge of the warm Southwestern US lower troposphere is more dominant across California during wildfire days leading to higher temperatures and less synoptic ventilation.

285   We summarize the characteristic value of daily maximum temperature (T_{max}), relative humidity (RH), specific humidity (q), scalar-mean windspeed (U), 24-hr $PM_{2.5}$, MDA8 O_3, CO and NO_x for wildfire and background days at each site in Fig. 3. The error bars show the interquartile range limited by 25th and 75th percentiles, and the center mark denotes the median value. For 24-hr $PM_{2.5}$ and CO, concentrations on wildfire days are significantly higher than non-fire days at all sites, since fine particles and CO are major products of biomass burning and are also good tracers of wildfire smoke. On average, the 24-hr

290    $PM_{2.5}$ and CO are 8.7 µg/m^3 (~102%) and 76 ppb (~4748%) higher than background periods, respectively. For most sites, the 25th percentile of the wildfire value is higher than the 75th percentile of non-fire periods. The clear difference in the concentrations of $PM_{2.5}$ and CO between wildfire and background days suggest that our wildfire identification method using the HMS system in conjunction with the HYSPLIT back-trajectory model can appropriately detect the presence of wildfire smoke at surface levels. It also suggests that our identification method has a similar effectiveness compared to methods that

295   use the HMS system and background $PM_{2.5}$ or CO as a threshold (e.g., mean background values plus one standard deviation) for wildfire identification in previous studies (McClure et al., 2018; Briggs et al.,2016). The MDA8 O_3 and NO_x concentrations are also enhanced during fire days by 6.5 ppb (~12%) and 0.9 ppb (~3532%) on average. The histograms in Fig. B1 show that about 289% and 40% of the wildfire-influenced days exceed the NAAQS of 70 ppb MDA8 O_3 versus only 123% and 16% during background periods for SV and SJV, respectively. The numbers and percentages of MDA8 O_3

300   exceedances of 70 ppb at each site are presented in Table C4. Overall, the wildfire events contribute to about 44% of the total exceedance cases. Using a global chemical transport model Pfister et al. (2008) estimated that the MDA8 O_3 increased by about 10 ppb on average for all sites in California during the wildfire events in the Fall (September to December) of 2007. Note that our study focuses only on the CV region in the summer months a decade later when the ambient NO_2 levels have decreased by approximately 50% in large urban areas (Simon et al., 2015) in California, and the model of Pfister et al. (2008)

305   exhibits biases in MDA8 O_3 of 10-15 ppb in fire and background conditions. Moreover, Figure 3 shows that the MDA8 O_3 has a southward directed gradient, in general, with higher O_3 concentration in the SJV than in the SV independent of whether or not wildfire emissions are present. This result is consistent with the EPA Green Book and the study conducted by Trousdell et al. (2019), in which they find that O_3 pollution in the SJV is still a problematic issue.

~~Figure 3: Median values for fire (red triangle) and non-fire (black circle) periods at each station, error bars represent 25th and 75th percentile values.~~
310   ~~RH, q, U, CO and NO_x are 5-hour averaged values between 10:00 to 15:00 PST. The interval of station-axis labeling is scaled to the latitude of each site.~~

    For meteorological factors, all sites except Chico show a higher median value (~0.5K on average) of T_{max} on wildfire influenced days. The result of higher temperature matches the previous long-term climatology studies on wildfire in U.S. from 1971 through 1984 (Potter, 1996), in which they report that wildfire events correspond to positive temperature anomalies. Brey et al. (2018) also show that in Mediterranean California, the temperature is positively correlated with

315   human-ignited burn area and the precipitation and RH are negatively correlated with both of human-ignited and lightning-ignited area, though the Pearson correlations are relatively smaller in California than other regions. The study of Brey et al. (20202021) found that in California's mountain regions, using wind speed, RH, and vapor pressure deficit (VPD) as the

11

predictors of wildfire burn areas yield ubiquitously small coefficients, and that only when RH is excluded as a predictor does the coefficient for summer VPD become appreciable in both historical data and future projections. However, in our study, a consistently higher specific humidity (q) is observed at all sites during wildfire periods by 0.6 g/kg on average. Additionally, higher RH values are also detected at most sites except for Merced and Bakersfield. The higher water vapor content observed in the valley ABL during wildfire periods is most likely not attributable to the chemical product of fuel combustion in the wildfires because that contribution would be stoichiometrically similar to CO_2 which is only observed to be enhanced by order of ~10 ppmv in such environments (Langford et al., 2020). Furthermore, the surface wind speeds show a reduction of about 0.3 m/s on average during wildfire periods at most sites except for Madera and Fresno. Thus, we hypothesize that the higher water vapor content and lower wind speeds are the result of weaker ABL entrainment due to the shading effect from wildfire plumes because of the reduced surface heat fluxes. This will be discussed further in section 3.3.
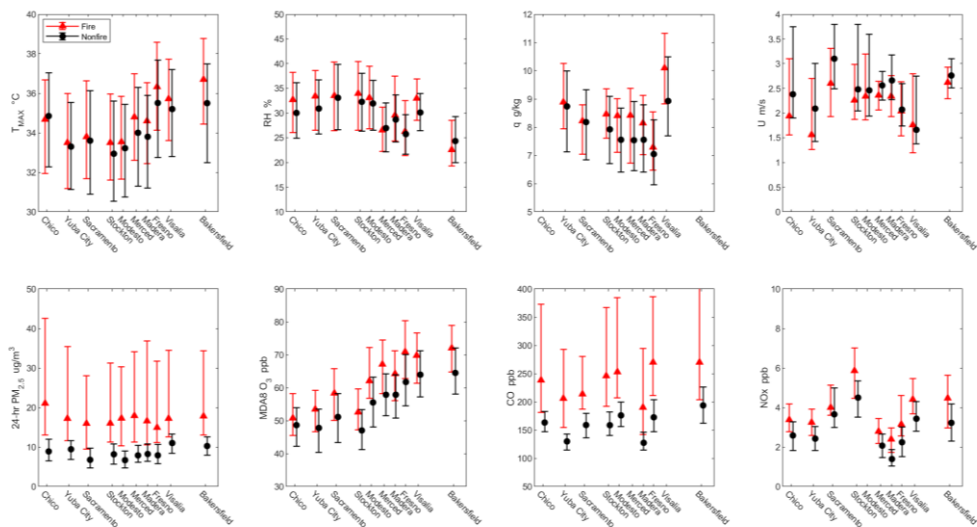
Figure 3: Median values for fire (red triangle) and non-fire (black circle) periods at each station, error bars represent 25th and 75th percentile values. RH, q, U, CO and NO$_x$ are 5-hour averaged values between 10:00 to 15:00 PST. The interval of station-axis labeling is scaled to the latitude of each site. The number of data points within each error bars are the same as the number of wildfire days and background days shown in Table C2, unless there are missing data.

We note that the O_3 concentrations have a relatively strong correlation with ambient temperature (Fig. B2) thus this meteorological variation needs to be considered when we analyze the O_3 enhancement (i.e., enhancement ratios for O_3 and temperature). According to Pusede et al., 2014, a study of daily maximum temperature versus daytime (10:00-14:00 local time) O_3 concentrations in Bakersfield, CA show the change of O_3 concentration with respect to temperature variation ($\Delta O_3/\Delta T_{max}$) to be around 2 ppb/K. Steiner et al. (2010) report O_3-temperature slopes of 2.4 ppb/K and 1.8 ppb/K in SJV and SV, respectively, yet their data is already a decade old, and they found that these slopes had been decreasing over the 30

12

years of their study. Our study (Fig. B2) shows that $\Delta O_3/\Delta T_{max}$ is on average 1.7 ppb/K for the background periods in the SJV and 1.3 ppb/K in the SV, consistent with a continued decrease in this parameter over time. Moreover, we found that the average slopes increase in the presence of wildfire emissions to 2.2 ppb/k (SJV) and 1.6 ppb/K (SV) also consistent with its dependence on precursor emissions (Sillman & Sampson, 1995). Thus, with an average of 0.5 K increase in temperature (T_{max}), we expect that approximately 1 ppb of the observed O_3 enhancement is due to the temperature increment during wildfire periods and the rest, 5.5 ppb of O_3 enhancement, is due to the influences of wildfire smoke. We also found that the ERs for $\Delta PM_{2.5}/\Delta CO$ have a strong positive correlation at all ten sites (Fig. B3), indicating that the $PM_{2.5}$ and CO are well connected to wildfire influence. Our average ER for $\Delta PM_{2.5}/\Delta CO$ (m value in Fig. B3) is 0.12 ($\pm$0.03) $\mu g/m^3$ ppb^{-1}, which agrees well with the value (0.107) found by Selimovic et al. (2019) in a study from two summers in Missoula, Montana as well as the value (0.12) reported by McClure and Jaffe (2018) from wildfires in Idaho.

3.2 Wildfire smoke influences on PM and O_3 production

In order to investigate the O_3 variations and their relationship to the existence of additional PM from wildfire smoke, we plot the binned 24-hr $PM_{2.5}$ versus corresponding MDA8 O_3 in Fig. 4. Since O_3 enhancements react differently across the CV, we separate our sites into two geographical categories: Chico, Yuba City and Sacramento into Sacramento Valley (SV) (Fig. 4(b)) and the remaining sites to the south into the SJV (Fig. 4(c)). Generally, MDA8 O_3 increases with PM at low 24-hr $PM_{2.5}$ concentrations for both the wildfire and background periods, peaking around 40 to 55 $\mu g/m^3$, then becomes independent of PM at higher concentration ($PM_{2.5}$ >55 $\mu g/m^3$). The slopes of the O_3 to $PM_{2.5}$ relationship (below 40 $\mu g/m^3$) are higher in the SJV than the SV. The non-linear relationship in our results generally aligns with the results from previous studies (Buysse et al.,2019; McClure et al., 2018), in which an increase of MDA8 O_3 with PM is found at low to moderate PM with a peak of MDA8 O_3 around 40 to 55 $\mu g/m^3$. However, our results do not show a clear decreasing trend of MDA8 O_3 at higher PM. The MDA8 O_3 did slightly decrease when $PM_{2.5}$ exceed 55 $\mu g/m^3$ in SJV, but it returns to its peak value when $PM_{2.5}$>100 $\mu g/m^3$.
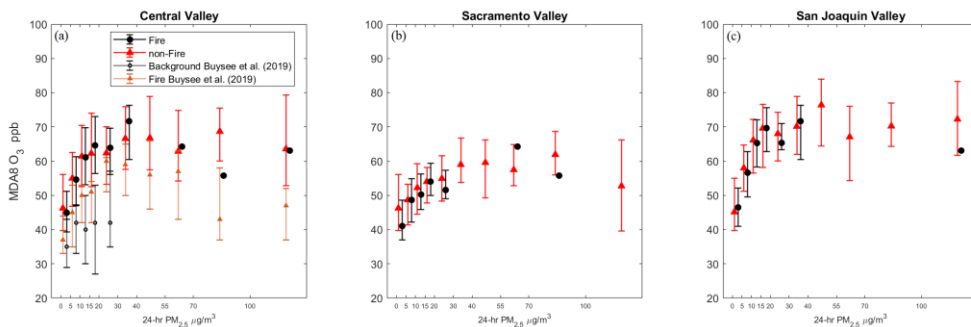
Figure 4: Plots for binned 24-hr $PM_{2.5}$ versus MDA8 O_3 for all ten sites (a); Chico, Yuba City, and Sacramento are in (b); and all other sites in the SJV in (c), black dots and red triangles denote median value for background and wildfire period, respectively. Error bars denote 25th and 75th percentile values. The number of datapoints in each bin can be found in Table C3. The orange (fire) and grey (non-fire) error bars are the result from Buysee et al. (2019) for comparison.

The NO levels, estimates of O_3 production raterates (PO$_3$),) and their dependence on the effective first-order reaction rate k[RO$_x$] (s^{-1}), NO, andNO$_2$ correction, along with the attenuation of incoming solar radiation are shown separately in Fig. 5.

365 The peak value of solar radiation (Fig. ~~5(d))~~5d) decreases by 7% on average at all ten sites during the wildfire periods. The ~~PO₃~~P(O₃) (Fig. ~~5(c)) that is calculated~~5c) estimated from the modified Leighton ratio increases at all sites during the wildfire influenced periods. ~~Despite the diminution of *j*(NO₂) due to the shading effect of wildfire smoke, the PO₃ increases by 26% (average of each site's enhancement ratio.) The rate k[ROₓ] (s⁻¹) (Fig. 5(b)) does not show a consistent enhancement pattern among all ten sites, but overall is enhanced by 11%. Figure 5(a) shows the NO concentrations are on average 0.07 ppb (19%)~~

370 ~~higher during wildfire periods, though two sites show negative increments. However, despite the variances of NO and k[ROₓ] at different sites, all sites have an enhancement of in-situ PO₃, which implies that the role of wildfire smoke is to provide additional NO, RO₂ and HO₂ to the O₃ photochemical cycle. The PO₃ and k[ROₓ] that are estimated from the modified Leighton ratio in our study tend to be higher than measured or modeled values (Pusede et al., 2014; Tan et al., 2018). Volz-Thomas et al. (2003) also used a modified Leighton ratio to estimate PO₃ and their results yielded up to 90~~

375 ~~ppb/h, which is similar to the magnitude of our results. They also calculate PO₃ from measured peroxy radicals and the result was much lower, around 10 ppb/h. There is a well-established record of the modified Leighton ratio method leading to significant overprediction of RO₂+HO₂ levels and thus implied photochemical ozone production rates (Volz-Thomas et al., 2003; Mannschreck et al., 2004; Griffin et al., 2007; Trousdell et al., 2019) for reasons that are not understood. We therefore do not expect this method to be accurate in this study, but we do believe that the results are still instructive in analyzing the~~

380 ~~relative changes in P(O₃) and [HO₂] + [RO₂] during wildfire and background periods. Overall, the relative increases in P(O₃) of ~26% during wildfire periods imply that O₃ enhancements are due to both increased peroxy radicals (or VOC precursors) and NO in approximately equal measure (11% and 19% increases respectively.) Although at some sites NO enhancements overwhelmed a dip in ROₓ (Madera & Visalia), and at others elevated ROₓ overwhelmed a smaller drop in NO (Merced & Bakersfield) all expressed elevated P(O₃). Using these measurements, it is impossible to know whether the enhancements in~~

385 ~~ROₓ under wildfire influence are generated from transported VOCs or partially oxidized VOCs or from thermally dissociated PAN transported to the sites in the fire plumes. Furthermore~~*j*(NO2) due to the shading effect of wildfire smoke, and the general enhancements of NO and O₃, the P(O₃) increases by up to ~50% (derived as the ratio of the valley-wide P(O3) averages in wildfire vs. background conditions). The uncorrected, fully corrected, and 20% intermediate stages of NO₂ correction are illustrated in Fig. 5b in order to represent the sensitivity of P(O₃) to our NO₂ correction magnitude separated into background (black) and wildfire (red) data. On average, the P(O₃) changes linearly by about 30 ppb/h for 1 ppb of NO₂

390 correction, and there is no significant difference in slope between wildfire and background conditions (29.1 vs 31.0). In the full correction, only one site, Bakersfield, shows a negative median value of P(O₃) for background days, but the valley-wide average is 18.7 ppb/hr. We consider this a very noisy measurement, but that some meaning can be retrieved in the valley-wide average. In order to contextualize these estimates, we present a summary of the midday P(O₃) values that have been

395 reported in the literature for the Southern San Joaquin Valley (SSJV) in Table 2.

Table 2: A summary of reported midday ozone photochemical production rates in the Southern SJV

Study	Year of data	Average [NOₓ] (ppb)	P(O₃) (ppb/hr)
Brune et al. (2016)	2010 (Bakersfield)	7	[7-12]
Trousdell et al. (2016)	2013/14 (Bakersfield)	4	8.2, [4-12]
Pusede et al. (2016)	2010 (Bakersfield)	2.3 (weekend)	[12-15]
Pusede et al. (2016)	2010 (Bakersfield)	5.3 (weekday)	[10-26]

14

| Trousdell et al. (2019) | 2016 (Fresno-Visalia) | 8 | 7, [2-14] |
| Ninneman & Jaffe (2021) | 2018 (Bakersfield) | 6 | 7, 12 (wildfires) |

Realizing that this study found the average NO_x to be only ~ 3 ppb, and that the NO_2/NO photostationary state method is known to overestimate $P(O_3)$ by about 2.5 times (Mannschreck et al., 2004), we can crudely surmise that the values we estimate should be in the range of about 10 – 20 ppb/hr, and thus the correction of Steinbacher et al. (2007) is most likely accurate to within ~ 30%. Further, assuming that the NO_2 corrections in the presence of fire smoke are most likely larger than those used here (from the average conditions of Steinbacher et al. (2007)), we infer that the average influence of wildfires in the Central Valley is to enhance in-situ ozone production rates by at most 50% (18.7 ppb/hr to 28.3 ppb/hr), and consider this to be an upper limit of enhancement. Although we acknowledge the large uncertainty in this modified Leighton method, we do believe that the results are still instructive in analyzing the relative changes in $P(O_3)$ during wildfire and background periods indicating that despite the 7% decrease in photolysis rates and enhancements in O_3 + NO reaction rates, ozone production increases up to 50% in wildfire conditions. Finally, any additional NO_y interference that is not fully corrected for by the Steinbacher et al. (2007) formula is likely due to the presence of oxidized nitrogen species originating from the wildfires and thus has contributed to the ozone enhancement somewhere along its path from the fire to the urban monitoring site even if it is not concurrently increasing the in-situ photochemical production rate.
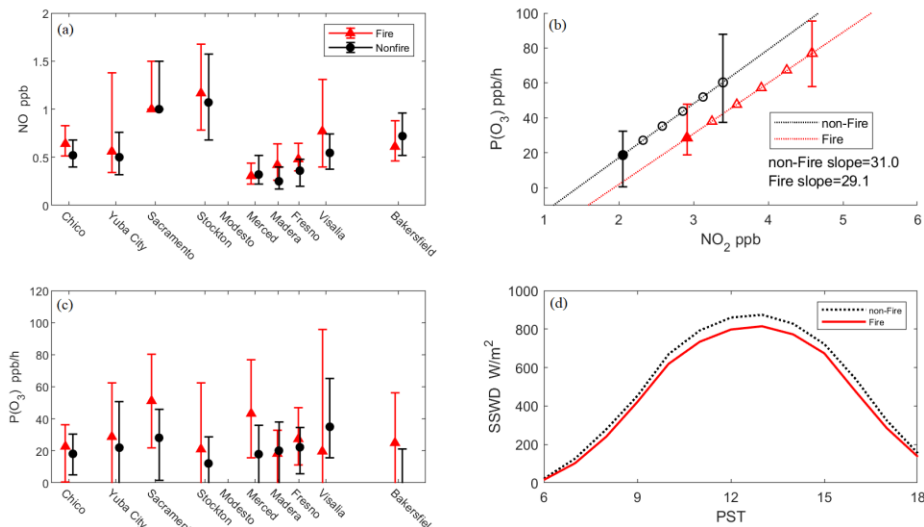

Figure 5: Plots ~~for~~**of (a)** NO measurements ~~(a),~~**, (b)** calculated ~~effective first-order reaction rate k[RO_x] (s⁻¹) (b),~~ $P(O_3)$ (ppb/h) at each stage of NO_2 correction (0-20%-40%-60%-80%, open, and 100%, solid), **(c)** calculated median PO_3 ~~(c)~~ at each site, and **(d)** averaged diurnal profiles for SSWD measurements ~~(d)~~. The error bars in (a), (b) and (c) represent 25th and 75th percentiles for 5-hour average between 10:00 and 15:00 PST during wildfire (red) and background (black) days.

15

O$_3$ production efficiency (OPE) is defined as the enhancement of O$_x$ (O$_3$+NO$_2$) with respect to NO$_z$ (NO$_y$-NO$_x$). It describes the amount of O$_3$ that is produced per NO$_x$ molecule consumed (Lin et al., 1988; Liu et al., 1987; Olszyna et al., 1994; Trainer et al., 1993). Figure 6 shows scatter plots for O$_x$ vs. NO$_z$ in ~~Sacramento (SV) and~~ Fresno (SJV) during the 2016-2020 O$_3$ seasons for both wildfire and background data. The slope value (m) is the enhancement of O$_x$ with respect to

420 NO$_z$ or OPE. ~~First, we found that the OPE in Sacramento is less than half that in Fresno despite the NO$_x$ levels being comparable (and even slightly larger in the background data set). This is consistent with the photochemical environment in the SJV having higher VOCs and thus behaving in a more NO$_x$-limited manner than the SV. Second, neither site shows a significant change in OPE~~ <u>Overall, the OPE does not show significant changes</u> when impacted by wildfires. The OPE is known to monotonically decrease with increasing NO$_x$ and increase with VOCs under most conditions (Lin et al., 1988;

425 Sillman, 1999). Thus, the insignificant changes in OPE ~~indicates~~<u>indicate</u> that the enhanced ozone level ~~throughout the CV~~<u>in SJV</u> are likely due to the concomitant presence of additional VOCs/RO$_x$ and NO$_x$ in approximately comparable measures.
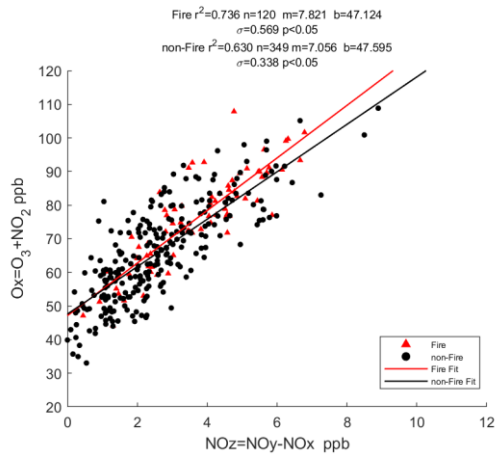

Fire r^2=0.736 n=120 m=7.821 b=47.124
σ=0.569 p<0.05
non-Fire r^2=0.630 n=349 m=7.056 b=47.595
σ=0.338 p<0.05

Figure 6: Scatter plot of O$_x$ versus NO$_z$ at ~~Sacramento (a) and~~ Fresno ~~(b)~~. The slope of the linear regression (m) represents the
430 **OPE. n is the number of data points in the scatter plot, σ is the standard error for the linear regression, and p is the P-value that**
represents the rejection of the null hypothesis. In this case, the P-values are less than 0.05, which we interpret as the regressions
being statistically significant.

3.3 Wildfire smoke's influence on boundary layer dynamics

Measurements of surface heat fluxes (Q_H, Q_E, and $\overline{w'\theta_v'}$) and SSWD at Twitchell Wetland (bottom) and Vaira Ranch
435 (top) are shown in Fig. 7. Both the sensible heat flux Q_H and buoyancy flux $\overline{w'\theta_v'}$ decrease during the wildfire periods, especially at Twitchell Wetland, where $\overline{w'\theta_v'}$ and Q_H are only about half as large on background days. The peak value of Q_E at Vaira Ranch decreases by 20 W/m^2 but increases by 20% on average at Twitchell Wetland. Note that, due to the difference in land types, the soil moisture is significantly higher in Twitchell than Varia, which explains the significantly smaller Q_E in

16

Vaira Ranch compared to Twitchell Wetland with a Bowen ratio of 11.7 and 0.6, respectively. Furthermore, the augmented

440   latent heat fluxes at Twitchell Wetland despite the reduced SSWD during wildfire conditions is consistent with an 'oasis effect' observed at the site wherein horizontal advection of warmer/drier air enhances evapotranspiration (Baldocchi et al., 2016). Across all sites, the reduced SSWD , Q_H, and $\overline{w'\theta_v'}$ below wildfire plumes will weaken the turbulent mixing within the ABL, reducing the ABL growth rate and height, which in principle would enhance the specific humidity and weaken the surface wind speed because a reduced buoyancy source of turbulent kinetic energy (TKE) will reduce the entrainment fluxes

445   of dry, higher momentum air across the inversion. Our results are consistent with the LES study of aerosol loading in the ABL by Liu et al. (2019), which showed that as aerosol optical depth (AOD) increases, less solar radiation reaches the surface, reducing the surface buoyancy flux, and weakening the entrainment.
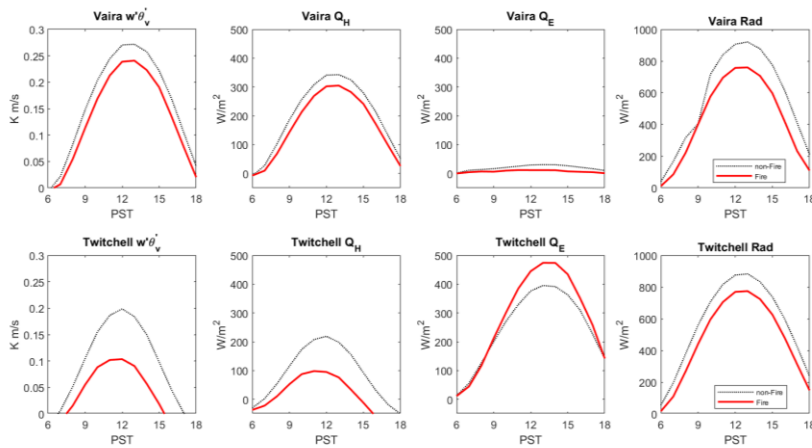
450   **Figure 7: Measurements of buoyancy flux ($w'\theta_v'$), sensible heat flux (Q_H), latent heat flux (Q_E), and incoming solar radiation (SSWD) at Vaira Ranch (top row) and Twitchell Wetland (bottom row). Red solid lines are averaged profiles during wildfire periods (Jun-Sep) from 2016 to 2019. Black dash lines are the averaged profile for non-fire days.**

    In order to visualize the condition of a polluted ABL during wildfire-influenced periods, Fig. 8 presents the daily averaged aerosol backscatter profiles during wildfire days (a) and background days (b) observed during the California

455   Baseline Ozone Transport Study (Faloona et al., 2020; Langford et al., 2020). The aerosol backscatter profiles are measured by a Tunable Optical Profiler for Aerosol and Ozone lidar (TOPAZ) that was located in Visalia, CA. During the wildfire periods, the backscatter is seen to be much greater in and above the ABL compared with the background days. We also show the averaged afternoon (13:00 to 15:00 PST) vertical profiles of backscatter in Fig. 8(c), where the aerosol load (i.e., backscatter β) is nearly doubled within the ABL (typically found up to ~600 m) during wildfire days. Figure 9(a) shows the

460   profiles of virtual potential temperature (θ_v) measured by the RASS located in Visalia. The profile is averaged from 13:00 to 15:00 PST during the summers of 2016-2020 for wildfire days (red) and background days (black) because daily maximum ABL height usually occurs around 14:00 in SJV (Bianco et al., 2011). The θ_v within the entire ABL is consistently about 1 –

17

2 K higher during wildfire days, and the warming is also apparent well above the ABL, which implies that aerosols within the lower valley atmosphere from wildfire plumes absorb solar radiation and warm the ABL and the buffer layer above it without appreciably influencing the stability per se. Liu et al. (2019) also simulate a warmer ABL with aerosols present in their LES, and potential temperature increasing with AOD. While we cannot be certain that the warmer lower troposphere under wildfire influence is solely due to shortwave absorption as opposed to simply climatological differences between wildfire and non-wildfire periods, we do know that surface SSWD and surface heat fluxes are reduced, so the enthalpy difference would likely be found in the lower troposphere. Assuming the 54 Wm^{-2} difference was fully absorbed in the lower 2 km of the valley atmosphere over the course of 8 hours this would lead to a heating of ~0.8 K. Furthermore, a study by David et al. (2018) ~~show~~shows that over a 6-year period in Northern California that wildfire smoke systematically lowers the SSWD by about 120 Wm^{-2} and raises the surface air temperature by about 1 K for each increase in AOD of 1. The 5-year averaged diurnal ABL height comparison between wildfire periods and background days is shown in Fig. 9(b) with SSWD comparison shown in Fig. 9(c). The midday ABL height is reduced by 80 m and the SSWD by about 54 W/m^2, on average. Pal and Haeffelin (2015) reported the slope for SSWD versus daily maximum ABL height to be 1.73 m/Wm^2 from an observatory outside of Paris, and Trousdell et al. (2016) report a similar slope of 1.51 m/Wm^{-2} in the SJV. In this study, the observed reduction in ABL height and SSWD due to the wildfire shading effects shown in Fig. 9 (80 m/54 Wm^{-2} = 1.48 m/Wm^{-2}) is quantitatively similar to the relationship between ABL height and SSWD in these other studies. It is also worthwhile noting that the altitude of highest backscatter gradient, which is another indicator of ABL height apart from the inversion of θ_v (Hennemuth et al., 2006), is actually lower during wildfire days (~550m) than on background days (~650m). The lowered backscatter inversion also illustrates that the ABL height is stunted due to the shading effect of the wildfire smoke plume. Since the wildfire plumes will weaken the entrainment at the ABL top and lower the ABL height, the rate of dilution from the buffer layer into the ABL and the volume for pollutant dispersion will also be reduced. Thus, the phenomenon of higher water content and lower wind speed described in section 3.1 could also be the consequence of weaker turbulent mixing within the ABL and the lower ABL heights observed during the wildfire days.
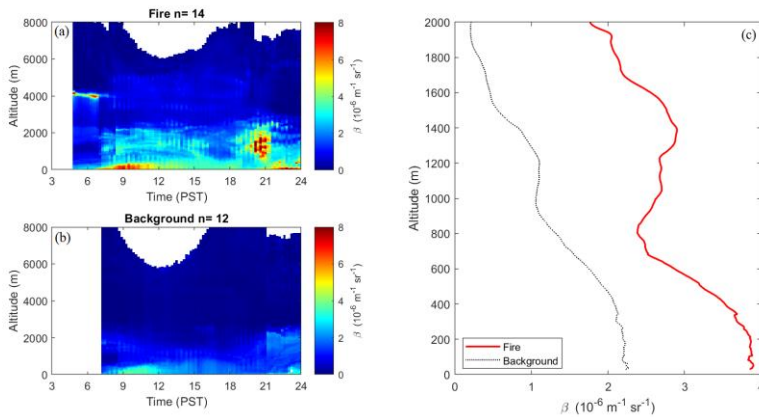

Figure 8: Aerosol backscatter profile for TOPAZ during CABOTS 2016. The plots are averaged diurnal profile for wildfire days (a) and background days (b) during 18 July to 7 August 2016. Averaged vertical backscatter profiles for

wildfire days (red) and background days (black) between 13:00 and 15:00 PST are in (c). n is the number of days in the average in each plot. The TOPAZ produces a vertical profile for every 12 mins with a resolution of 5m.

490   Therefore, the wildfire smoke plays two distinct roles in influencing the ABL dynamics and scalar budgets. First, by attenuating surface insolation the smoke reduces the surface heat fluxes weakening ABL entrainment thereby decreasing the maximum ABL height, decreasing ABL wind speeds, and increasing water vapor mixing ratios. The weakened entrainment will likely affect other scalars that are strongly influenced by entrainment dilution such as methane (Trousdell et al., 2019), N_2O, and CO_2 all else being equal; however, these trace gases are likewise influenced by wildfire emissions, so the impacts

495   are more complex. Second, the smoke absorbs solar radiation warming the air in the ABL (and above) thereby offsetting the reduced surface and entrainment heat fluxes in terms of its impact on air temperature.
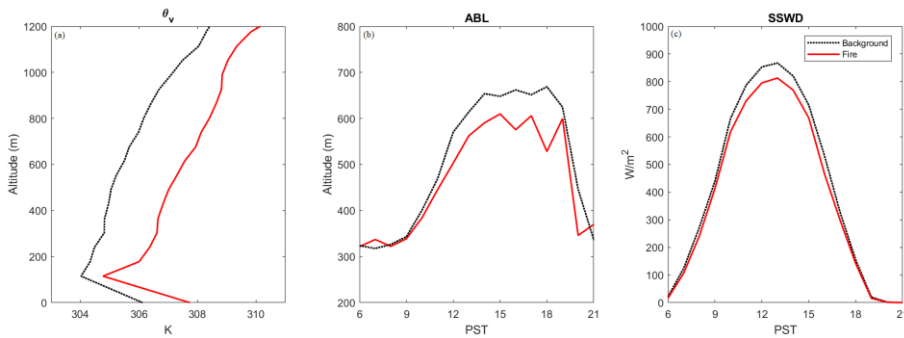
Figure 9: Averaged virtual potential temperature (θ_v) profile between 13:00 and 15:00 PST (a), diurnal profile for daytime ABL height (b), and diurnal SSWD profile (c) at Visalia during wildfire days (red) and background periods (black) from 2016 to 2020.

4   Conclusions

500   O_3 pollution is still an issue in California's urban regions during summer seasons when wildfires are also prone to happen, and ~~which~~ are becoming larger and more frequent. The wildfires can not only emit primary pollutants like, CO, NO_x, black carbon, volatile organic compounds, and fine particles, but also provide reactants for the production of secondary pollutants like O_3. We use data from ten sites in California's Central Valley region during the summers from 2016-2020 and identified wildfire events by the HMS system and HYSPLIT modeling. On average, the wildfire influenced days in the CV add up to

505   about 20% of the entire summer time (~120 days out of 600 days). During these periods we found that MDA8 O_3 increases by 6.5 ppb on average with about 5.5 ppb ~~(~~(+10%) being attributable to the wildfires after correcting for the bias in temperature for wildfire conditions. Further, NO_x concentrations during daytime increase by up to 0.9 ppb (~~35~~32%) and CO is higher on average by 76 ppb (48%). The MDA8 O_3 increases with 24-hr $PM_{2.5}$ at low to moderate concentrations, peaks at 40-55µg/m^3, and is more or less independent of $PM_{2.5}$ at higher concentrations. From our 5-year data analysis, the probability

510   of exceeding the NAAQS of 70 ppb MDA8 O_3 is more than doubled (~~28~~9% and 40%) during wildfire ~~influence~~ influenced periods compared to background periods (~~12%)~~3% and16%) for SV and SJV, respectively. The wildfire events contribute to about 44% of the total exceedance cases. Daily maximum temperature and specific humidity show enhancement at most sites (averages of +0.5K and +0.6 gkg^{-1}), whereas midday windspeed is slightly decreased. The in-situ $P(O_3)$ exhibits enhancement

19

at all ~~sites~~ stages of NO_2 correction, and by an average of ~~25~~up to ~50%, despite $j(NO_2)$ being reduced due to the shading effect of the wildfire plumes. The analysis indicates that $P(O_3)$ would change significantly with the uncertainties of NO_2 measurement (~30 ppb/h $P(O_3)$ per ppb NO_2), which suggests that accurate measurements of NO_2 are crucial to accurately estimating $P(O_3)$ by using the modified Leighton relationship. Nevertheless, our results still show distinctive differences of the $P(O_3)$ between wildfire and background periods, even with relatively large uncertainties in the NO_2 measurements. The OPE ~~is slightly enhanced by ~10%~~has insignificant changes in the SJV ~~and unchanged in the SV~~ despite the increase in NO_x during wildfire influence from which we conclude that both the VOCs, and their oxidation products, and NO_x from wildfire plumes contribute to increasing O_3 production.

We analyze surface heat flux measurements from two AmeriFlux sites located in the northern SJV and ABL temperature profiles and ABL heights from a RASS site near Visalia. We find that the surface buoyancy flux decreases by an average of 30% when overhead wildfire plumes are detected. We also find that the midday ABL height decreases by 80 m on average with an attenuation of 54 W/m^2 in SSWD. Despite the decreased surface buoyancy fluxes, the θ_v measurements from RASS show that the ABL becomes 1-2 K warmer on average during wildfire influenced periods. This implies that the ABL dynamics will change due to the presence of wildfire plumes and are the net result of two factors. First, the shading effect of the wildfire plumes decreases the SSWD, surface heat fluxes, and consequently reduces the ABL height. Second, the additional aerosols in the ABL absorb solar radiation and warm the ABL as well as the 'buffer layer' above it. Since the turbulent entrainment mixing into the ABL and the height itself have critical impacts on the concentration budgets of constituent (e.g., pollutants, water vapor), the weakened turbulent mixing and lowered ABL height will serve to make an already polluted ABL even worse.

Appendices:

The equation for j(NO_2) calculation from surface solar radiation measurements (Trebs et al., 2009).

$$j(NO_2) \downarrow = B_1 \times G + B_2 \times G^2 \tag{A1}$$

Where B_1=1.47*10^{-5} $W^{-1}m^2s^{-1}$ and B_2=-4.84*10^{-9} $W^{-1}m^2s^{-1}$ are polynomial coefficients, G is solar radiation measurement.

$$k_{O_3} = 3.47 \, \cancel{exp\left(-\frac{1533}{T}\right)} \times 10^{-12} \exp\left(-\frac{1533}{T}\right) \; cm^3/molecule \, \cancel{sec}$$

$$\text{(A2)}$$

Equation (A2) is the Arrhenius function to calculate k_{O_3} based on temperature T, the result derived from the function fits the experiment result extremely well through the common temperature range of 283-364K (Lippmann et al., 1980).
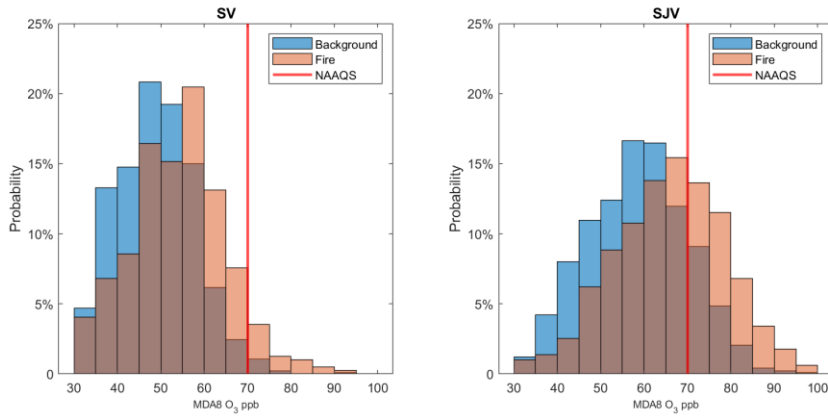
Figure B1. Histograms ~~for~~of **MDA8 O$_3$ for wildfire periods (orange)** ~~and~~overlay on **background periods (blue) during summer (Jun-Sep) from 2016 to 2020. The sites are sorted into SV (left) and SJV (right). During wildfire periods,** ~~almost 28~~about 9% and 40% **of the days exceed the NAAQS of 70 ppb MDA8 O$_3$ (red line)** ~~vs~~versus **only** ~~1~~23% and 16% **during background periods** for SV and SJV, respectively.
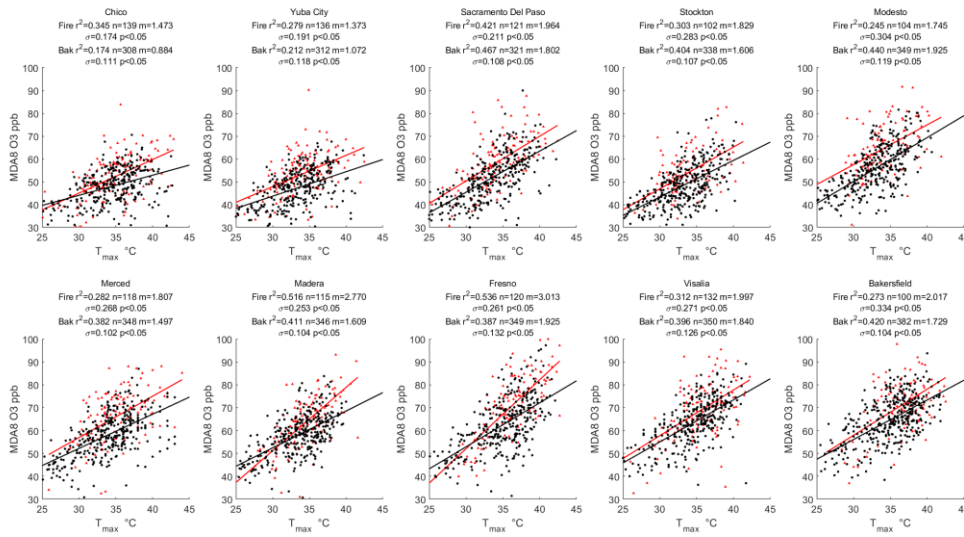
Figure B2. Scatter plot and linear regression for daily maximum temperature versus MDA8 O$_3$ at each site for wildfire periods (red) and background periods (black). The r^2 above each figure is the coefficient of determination, m is the slope or enhancement ratio, the n is the number of data points in the regression, the σ is the standard error for the linear regression, p is the P-value that represents the rejection of null hypothesis.
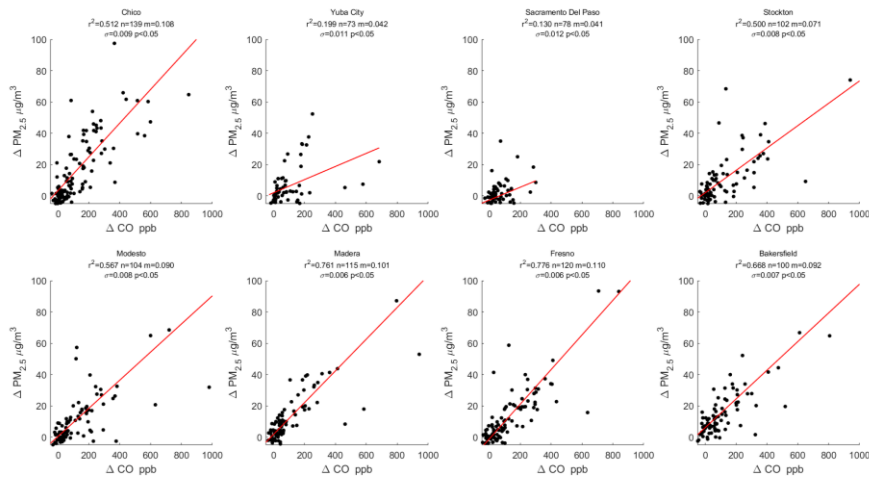
Figure B3. Scatter plot and linear regression for ΔPM₂.₅ versus ΔCO at each site. Enhancements are the differences in afternoon
(10:00-15:00 PST) mean values between wildfire and background periods. The m is the slope or enhancement ratio, the n is the
number of data points in the regression, the σ is the standard error for the linear regression, p is the P-value that represent the
rejection of null hypothesis.
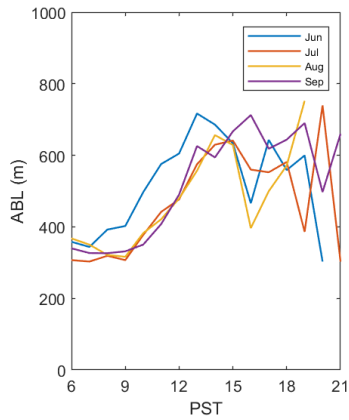
Figure B4. Monthly averaged diurnal ABL height during June to September from 2016 to 2020.
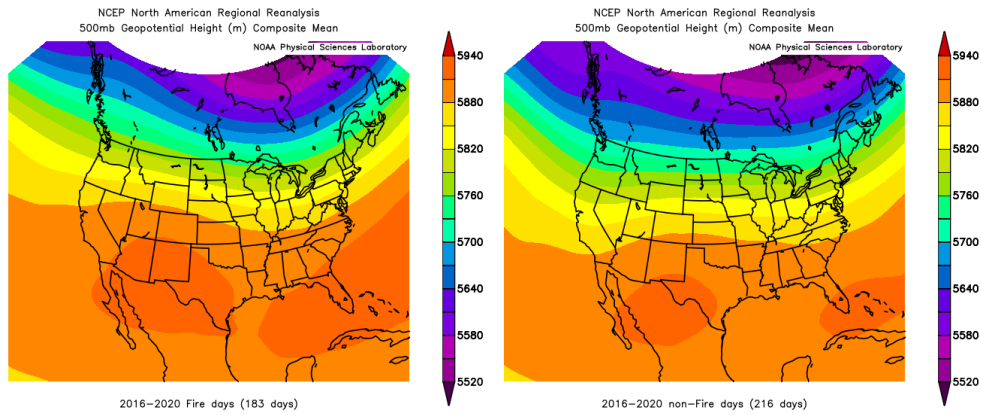
Figure B5. The composite means of 500mb geopotential height for wildfire (left) and background (right) days during summer 2016-2020 (NOAA Physical Sciences Laboratory, https://psl.noaa.gov/cgi-bin/data/getpage.pl).

Variables	Coefficient
Intercept (e)	-1.32E-1
$(NO2)_m$ (a)	1.32E-1
O3 (b)	2.71E-2
Month (c)	
Jan	0
Feb	-0.012
Mar	0.258
Apr	0.380
May	0.239
Jun	-0.092
Jul	-0.105
Aug	-0.135
Sep	0.050
Oct	-0.050
Nov	-0.274
Dec	-0.026
day (d)	-1.87E-1

Table C1. Constants in Eq. (6) for NO_2 correction (Steinbacher et al., 2007). The result is from the multiple linear regression model at Taenikon site.

575

24

Site	Wildfire Days	Background Days
Chico	139	308
Yuba City	136	312
Sacramento	121	321
Stockton	102	338
Modesto	104	349
Merced	118	348
Madera	115	346
Fresno	120	349
Visalia	132	350
Bakersfield	100	382

Table C2. Number of the wildfire influenced and background days at each site during summer (Jun-Sep) 2016-2020.

Inserted Cells

24-hr PM$_{2.5}$		CV	SV	SJV
< 5 µg/m^3	Fire	20	11	9
	Background	480	169	311
5-10 µg/m^3	Fire	200	66	134
	Background	1669	429	1240
10-15 µg/m^3	Fire	272	74	198
	Background	919	243	676
15-20 µg/m^3	Fire	182	61	121
	Background	229	67	162
20-30 µg/m^3	Fire	163	67	96
	Background	54	17	37
30-40 µg/m^3	Fire	125	34	91
	Background	6	0	6
40-55 µg/m^3	Fire	98	41	57
	Background	0	0	0
55-70 µg/m^3	Fire	34	11	23
	Background	1	1	0
70-100 µg/m^3	Fire	42	12	30
	Background	1	1	0
> 100 µg/m^3	Fire	39	12	27
	Background	1	0	1

Table C3. Number of data points in each bin in Fig. 4.

Formatted: Font: 10 pt, Not Bold

Formatted: Don't add space between paragraphs of the same style, Don't swap indents on facing pages

Site	Fire	Non-fire	Percentage of Fire
CHICO	4	1	80
YUBA CITY	4	0	100
SACRAMENTO	18	12	60
STOCKTON	6	5	55
MODESTO	29	33	47
MERCED	49	39	56
MADEARA	33	27	55
FRESNO	63	87	42
VISALIA	63	98	39
BAKERSFIELD	58	120	33
Total	327	422	44

595 **Table C4. Number and percentage of the exceedances of 70 ppb MDA8 O_3 at each site.**

Data Availability

All air quality and meteorological data (section 2.1) are download from Air Quality and Meteorological Information System of California Air Resources Board's (CARB) website.

600

NO_y data (section 3.2) are downloaded from AirNow-Tech website.

Solar radiation measurements (section 2.3) are download from CIMIS websites.

605 RASS data collected near Visalia (section 2.4) was downloaded from the website of NOAA's Physical Sciences Laboratory.

Surface fluxes data (section 2.4) of Twitchell Island and Vaira Ranch are downloaded from AmeriFlux website.

TOPAZ data from NOAA Earth System Research Laboratory Chemical Sciences Division during 2016 CABOTS are used in section 3.3.

610 **Competing Interests:**

The authors declare that they have no conflict of interest.

Acknowledgements

Formatted: Font color: Auto, Pattern: Clear

References

Ainsworth, E.: A. Understanding and improving global crop response to ozone pollution, The Plant Journal, 90(5), 886-897, https://doi.org/10.1111/tpj.13298, 2017.

AirNow-Tech: Data Queries, MADIS, https://www.airnowtech.org/data/index.cfm, 2020.

Akagi, S. K., Yokelson, R. J., Burling, I. R., Meinardi, S., Simpson, I., Blake, D. R., ... & Urbanski, S.: Measurements of reactive trace gases and variable O3 formation rates in some South Carolina biomass burning plumes, https://doi.org/10.5194/acp-13-1141-2013, 2013.

Alvarado, M. J., Logan, J. A., Mao, J., Apel, E., Riemer, D., Blake, D., ... & Wooldridge, P. J.: Nitrogen oxides and PAN in plumes from boreal fires during ARCTAS-B and their impact on ozone: an integrated analysis of aircraft and satellite observations, Atmospheric Chemistry and Physics, 10(20), 9739-9760, https://doi.org/10.5194/acp-10-9739-2010, 2010.

~~Arya, P. S.: Introduction to micrometeorology, Elsevier, 2001.~~

Baker, K. R., Woody, M. C., Valin, L., Szykman, J., Yates, E. L., Iraci, L. T., ... & Campuzano-Jost, P.: Photochemical model evaluation of 2013 California wild fire air quality impacts using surface, aircraft, and satellite data, Science of The Total Environment, 637, 1137-1149, https://doi.org/10.1016/j.scitotenv.2018.05.048, 2018.

Baldocchi, D., Knox, S., Dronova, I., Verfaillie, J., Oikawa, P., Sturtevant, C., ... & Detto, M.: The impact of expanding flooded land area on the annual evaporation of rice. *Agricultural and Forest Meteorology*, 223, 181-193, https://doi.org/10.1016/j.agrformet.2016.04.001, 2016.

Baylon, P., Jaffe, D. A., Hall, S. R., Ullmann, K., Alvarado, M. J., & Lefer, B. L.: Impact of biomass burning plumes on photolysis rates and ozone formation at the Mount Bachelor Observatory, Journal of Geophysical Research: Atmospheres, 123(4), 2272-2284, https://doi.org/10.1002/2017JD027341, 2018.

Baylon, P., Jaffe, D. A., Wigder, N. L., Gao, H., & Hee, J.: Ozone enhancement in western US wildfire plumes at the Mt. Bachelor Observatory: The role of NOx, Atmospheric Environment, 109, 297-304, https://doi.org/10.1016/j.atmosenv.2014.09.013, 2015.

~~Berkowicz, R., & Prahm, L. P.: Evaluation of the profile method for estimation of surface fluxes of momentum and heat, Atmospheric Environment (1967), 16(12), 2809-2819, https://doi.org/10.1016/0004-6981(82)90032-4, 1982.~~

27

Bianco, L., Djalalova, I. V., King, C. W., & Wilczak, J. M.: Diurnal evolution and annual variability of boundary-layer height and its correlation to other meteorological variables in California's Central Valley, Boundary-layer meteorology, 140(3), 491-511, DOI: 10.1007/s10546-011-9622-4, 2011.

650 ~~Brasseur, G. P., Orlando, J. J., & Tyndall, G. S.: Atmospheric chemistry and global change, (p. 654), New York: Oxford Univ. Press, 1999.~~

Brey, S. J., & Fischer, E. V.: Smoke in the city: how often and where does smoke impact summertime ozone in the United States?, Environmental science & technology, 50(3), 1288-1294, https://doi.org/10.1021/acs.est.5b05218, 2016.

Brey, S. J., Barnes, E. A., Pierce, J. R., Swann, A. L., & Fischer, E. V.: Past variance and future projections of the
655 environmental conditions driving western US summertime wildfire burn area. *Earth's future*, 9(2), e2020EF001645, https://doi.org/10.1029/2020EF001645, 2021.

Brey, S. J., Barnes, E. A., Pierce, J. R., Wiedinmyer, C., & Fischer, E. V.: Environmental conditions, ignition type, and air quality impacts of wildfires in the southeastern and western United States. Earth's future, 6(10), 1442-1456, https://doi.org/10.1029/2018EF000972, 2018.

660 Brey, S. J., Ruminski, M., Atwood, S. A., & Fischer, E. V.: Connecting smoke plumes to sources using Hazard Mapping System (HMS) smoke and fire location data over North America, Atmospheric Chemistry and Physics, 18(3), 1745-1761, https://doi.org/10.5194/acp-18-1745-2018, 2018.

Briggs, N. L., Jaffe, D. A., Gao, H., Hee, J. R., Baylon, P. M., Zhang, Q., ... & Cary, R. A.: Particulate matter, ozone, and nitrogen species in aged wildfire plumes observed at the Mount Bachelor Observatory, Aerosol and Air Quality
665 Research, 16(12), DOI: 10.4209/aaqr.2016.03.0120, 2016.

Brune, W. H., Baier, B. C., Thomas, J., Ren, X., Cohen, R. C., Pusede, S. E., ... & Wennberg, P. O.: Ozone production chemistry in the presence of urban plumes. *Faraday discussions*, *189*, 169-189, DOI: 10.1039/C5FD00204D, 2016.

Buysse, C. E., Kaulfus, A., Nair, U., & Jaffe, D. A.: Relationships between particulate matter, ozone, and nitrogen oxides during urban smoke events in the western US. Environmental science & technology, 53(21), 12519-12528,
670 https://doi.org/10.1021/acs.est.9b05241, 2019.

California Air Resources Board: Air Quality and Meteorological Information System, https://www.arb.ca.gov/aqmis2/aqmis2.php, 2020.

California Irrigation Management Information System: Solar Radiation Measurements, CIMIS Stations Reports, https://cimis.water.ca.gov/WSNReportCriteria.aspx, 2020.

675 David, A. T., Asarian, J. E., & Lake, F. K.: Wildfire smoke cools summer river and stream water temperatures. *Water Resources Research*, 54(10), 7273-7290, https://doi.org/10.1029/2018WR022964, 2018.

de Gouw, J. A., & Lovejoy, E. R.: Reactive uptake of ozone by liquid organic compounds, Geophysical Research Letters, 25(6), 931-934, https://doi.org/10.1029/98GL00515, 1998.

Dunlea, E. J., Herndon, S. C., Nelson, D. D., Volkamer, R. M., San Martini, F., Sheehy, P. M., ... & Molina, M. J.:
680 Evaluation of nitrogen dioxide chemiluminescence monitors in a polluted urban environment. *Atmospheric Chemistry and Physics*, 7(10), 2691-2704, https://doi.org/10.5194/acp-7-2691-2007, 2007.

Faloona, I. C., Chiao, S., Eiserloh, A. J., Alvarez, R. J., Kirgis, G., Langford, A. O., ... & Yates, E. L.: The California
Baseline Ozone Transport Study (CABOTS), Bulletin of the American Meteorological Society, 101(4), E427-E445,
https://doi.org/10.1175/BAMS-D-18-0302.1, 2020.

685 Fischer, E. V., Jaffe, D. A., Reidmiller, D. R., & Jaegle, L.: Meteorological controls on observed peroxyacetyl nitrate at
Mount Bachelor during the spring of 2008, Journal of Geophysical Research: Atmospheres, 115(D3),
https://doi.org/10.1029/2009JD012776, 2010.

~~Griffin, R. J., Beckman, P. J., Talbot, R. W., Sive, B. C., & Varner, R. K.: Deviations from ozone photostationary state
during the International Consortium for Atmospheric Research on Transport and Transformation 2004 campaign: Use of~~
690 ~~measurements and photochemical modeling to assess potential causes, Journal of Geophysical Research:
Atmospheres, 112(D10), https://doi.org/10.1029/2006JD007604, 2007.~~

Hazard Mapping System Fire and Smoke Product, https://www.ospo.noaa.gov/Products/land/hms.html, December 2020.

Hennemuth, B., & Lammert, A.: Determination of the atmospheric boundary layer height from radiosonde and lidar
backscatter. *Boundary-Layer Meteorology*, 120(1), 181-200, https://doi.org/10.1007/s10546-005-9035-3, 2006.

695 Jaffe, D. A., & Wigder, N. L.: Ozone production from wildfires: A critical review, Atmospheric Environment, 51, 1-10,
https://doi.org/10.1016/j.atmosenv.2011.11.063, 2012.

Jenkin, M. E., & Hayman, G. D.: Photochemical ozone creation potentials for oxygenated volatile organic compounds:
sensitivity to variations in kinetic and mechanistic parameters. *Atmospheric environment*, 33(8), 1275-1293,
https://doi.org/10.1016/S1352-2310(98)00261-1, 1999.

700 Langford, A. O., Alvarez, R. J., Brioude, J., Caputi, D., Conley, S. A., Evan, S., et al.: Ozone production in the Soberanes
smoke haze: Implications for air quality in the San Joaquin Valley during the California Baseline Ozone Transport Study,
Journal of Geophysical Research: Atmospheres, 125, e2019JD031777, https://doi.org/10.1029/2019JD031777, 2020.

Leighton, P. A.: Photochemistry of Air Pollution, Academic Press: New York, Vol. 9, 1961.

Leukauf, D., Gohm, A., & Rotach, M. W.: Quantifying horizontal and vertical tracer mass fluxes in an idealized valley
705 during daytime, Atmospheric Chemistry and Physics, 16(20), 13049, https://doi.org/10.5194/acp-16-13049-2016, 2016.

Lin, M., Horowitz, L. W., Payton, R., Fiore, A. M., & Tonnesen, G.: US surface ozone trends and extremes from 1980 to
2014: quantifying the roles of rising Asian emissions, domestic controls, wildfires, and climate, Atmospheric Chemistry
& Physics, 17(4), https://doi.org/10.5194/acp-17-2943-2017, 2017.

Lin, X., Trainer, M., & Liu, S. C.: On the nonlinearity of the tropospheric ozone production, Journal of Geophysical
710 Research: Atmospheres, 93(D12), 15879-15888, https://doi.org/10.1029/JD093iD12p15879, 1988.

Lippmann, H. H., Jesser, B., & Schurath, U.: The rate constant of NO+ O3→ NO2+ O2 in the temperature range of 283–443
K, International Journal of Chemical Kinetics, 12(8), 547-554, https://doi.org/10.1002/kin.550120805, 1980.

Liu, C., Fedorovich, E., Huang, J., Hu, X. M., Wang, Y., & Lee, X.: Impact of aerosol shortwave radiative heating on
entrainment in the atmospheric convective boundary layer: A large-eddy simulation study, Journal of the Atmospheric
715 Sciences, 76(3), 785-799, https://doi.org/10.1175/JAS-D-18-0107.1, 2019.

Liu, S. C., Trainer, M., Fehsenfeld, F. C., Parrish, D. D., Williams, E. J., Fahey, D. W., ... & Murphy, P. C.: Ozone
production in the rural troposphere and the implications for regional and global ozone distributions, Journal of
Geophysical Research: Atmospheres, 92(D4), 4191-4207, https://doi.org/10.1029/JD092iD04p04191, 1987.

Mannschreck, K., Gilge, S., Plass-Duelmer, C., Fricke, W., & Berresheim, H.: Assessment of the applicability of NO-NO 2-O 3 photostationary state to long-term measurements at the Hohenpeissenberg GAW Station, Germany. *Atmospheric Chemistry and Physics*, 4(5), 1265-1277, https://doi.org/10.5194/acp-4-1265-2004, 2004.

Mannschreck, K., Klemp, D., Kley, D., Friedrich, R., Kühlwein, J., Wickert, B., ... & Slemr, F.: Evaluation of an emission inventory by comparisons of modelled and measured emission ratios of individual HCs, CO and NOx, Atmospheric Environment, 36, 81-94. https://doi.org/10.1016/S1352-2310(02)00211-X, 2002.

Val Martín, M. V., Honrath, R. E., Owen, R. C., Pfister, G., Fialho, P., & Barata, F.: Significant enhancements of nitrogen oxides, black carbon, and ozone in the North Atlantic lower free troposphere resulting from North American boreal wildfires, Journal of Geophysical Research: Atmospheres, 111(D23), https://doi.org/10.1029/2006JD007530, 2006.

McClure, C. D., & Jaffe, D. A.: Investigation of high ozone events due to wildfire smoke in an urban area, Atmospheric Environment, 194, 146-157, https://doi.org/10.1016/j.atmosenv.2018.09.021, 2018.

National Report of Wildland Fires and Acres Burned by State, https://www.nifc.gov/fire-information/statistics, December 2020.

Ninneman, M., & Jaffe, D. A.: The impact of wildfire smoke on ozone production in an urban area: Insights from field observations and photochemical box modeling. *Atmospheric Environment*, *267*, 118764, https://doi.org/10.1016/j.atmosenv.2021.118764, 2021.

NOAA Physical Sciences Laboratory: 915 MHz Wind Profiler, Profiler Network Data & Image Library, https://psl.noaa.gov/data/obs/datadisplay/, 2020.

NOAA, Physical Sciences Laboratory: Climate Analysis and Plotting Tools, https://psl.noaa.gov/cgi-bin/data/getpage.pl, 2022.

Olszyna, K. J., Bailey, E. M., Simonaitis, R., & Meagher, J. F.: O3 and NO y relationships at a rural site, Journal of Geophysical Research: Atmospheres, 99(D7), 14557-14563, https://doi.org/10.1029/94JD00739, 1994.

Pahlow, M., Kleissl, J., & Parlange, M. B.: Atmospheric boundary-layer structure observed during a haze event due to forest-fire smoke, Boundary-layer meteorology, 114(1), 53-70, DOI: 10.1007/s10546-004-6350-z, 2005.

Pal, S., & Haeffelin, M.: Forcing mechanisms governing diurnal, seasonal, and interannual variability in the boundary layer depths: Five years of continuous lidar observations over a suburban site near Paris, Journal of Geophysical Research: Atmospheres, 120(23), 11-936, https://doi.org/10.1002/2015JD023268, 2015.

Parrish, D. D., Trainer, M., Holloway, J. S., Yee, J. E., Warshawsky, M. S., Fehsenfeld, F. C., ... & Moody, J. L.: Relationships between ozone and carbon monoxide at surface sites in the North Atlantic region, Journal of Geophysical Research: Atmospheres, 103(D11), 13357-13376, https://doi.org/10.1029/98JD00376, 1998.

Pfister, G. G., Wiedinmyer, C., & Emmons, L. K.: Impacts of the fall 2007 California wildfires on surface ozone: Integrating local observations with global model simulations, Geophysical Research Letters, 35(19), https://doi.org/10.1029/2008GL034747, 2008.

Potter, B. E.: Atmospheric properties associated with large wildfires, International Journal of Wildland Fire, 6(2), 71-76, https://doi.org/10.1071/WF9960071, 1996.

Pusede, S. E., Duffey, K. C., Shusterman, A. A., Saleh, A., Laughner, J. L., Wooldridge, P. J., ... & Cohen, R. C.: On the effectiveness of nitrogen oxide reductions as a control over ammonium nitrate aerosol. *Atmospheric Chemistry and Physics*, *16*(4), 2575-2596, https://doi.org/10.5194/acp-16-2575-2016, 2016.

30

Pusede, S. E., Gentner, D. R., Wooldridge, P. J., Browne, E. C., Rollins, A. W., Min, K. E., ... & Henry, S. B.: On the temperature dependence of organic reactivity, nitrogen oxides, ozone production, and the impact of emission controls in San Joaquin Valley, California, Atmospheric Chemistry and Physics, 14(7), 3373-3395, https://doi.org/10.5194/acp-14-3373-2014, 2014.

Reid, J. S., Koppmann, R., Eck, T. F., & Eleuterio, D. P.: A review of biomass burning emissions part II: intensive physical properties of biomass burning particles, Atmospheric Chemistry and Physics, 5(3), 799-825, https://doi.org/10.5194/acp-5-799-2005, 2005.

Rolph, G. D., Draxler, R. R., Stein, A. F., Taylor, A., Ruminski, M. G., Kondragunta, S., ... & Davidson, P. M.: Description and verification of the NOAA smoke forecasting system: the 2007 fire season, Weather and Forecasting, 24(2), 361-378. https://doi.org/10.1175/2008WAF2222165.1, 2009.

Rombout, P. J., Lioy, P. J., & Goldstein, B. D.: Rationale for an eight-hour ozone standard, Journal of the Air Pollution Control Association, 36(8), 913-917, https://doi.org/10.1080/00022470.1986.10466130, 1986.

Ruminski, M., Kondragunta, S., Draxler, R., & Zeng, J.: Recent changes to the hazard mapping system, In Proceedings of the 15th International Emission Inventory Conference, Vol. 15, p. 18, 2006.

Sara Knox, Jaclyn Hatala Matthes, Joseph Verfaillie, Dennis Baldocchi: AmeriFlux BASE US-Twt Twitchell Island, Ver. 6-5, AmeriFlux AMP, (Dataset), https://doi.org/10.17190/AMF/1246140, 2018.

Selimovic, V., Yokelson, R. J., McMeeking, G. R., & Coefield, S.: In situ measurements of trace gases, PM, and aerosol optical properties during the 2017 NW US wildfire smoke event, Atmospheric Chemistry and Physics, 19(6), 3905-3926, https://doi.org/10.5194/acp-19-3905-2019, 2019.

Selimovic, V., Yokelson, R. J., McMeeking, G. R., & Coefield, S.: Aerosol mass and optical properties, smoke influence on O3, and high NO3 production rates in a western US city impacted by wildfires, Journal of Geophysical Research: Atmospheres, 125(16), e2020JD032791, https://doi.org/10.1029/2020JD032791, 2020.

Sillman, S., & Samson, P. J.: Impact of temperature on oxidant photochemistry in urban, polluted rural and remote environments, Journal of Geophysical Research: Atmospheres, 100(D6), 11497-11508, https://doi.org/10.1029/94JD02146, 1995.

Sillman, S.: The relation between ozone, NOx and hydrocarbons in urban and polluted rural environments, Atmospheric Environment, 33(12), 1821-1845, https://doi.org/10.1016/S1352-2310(98)00345-8, 1999.

Simon, H., Reff, A., Wells, B., Xing, J., & Frank, N.: Ozone trends across the United States over a period of decreasing NOx and VOC emissions. *Environmental science & technology*, 49(1), 186-195, https://doi.org/10.1021/es504514z, 2015.

Singh, H. B., Cai, C., Kaduwela, A., Weinheimer, A., & Wisthaler, A.: Interactions of fire emissions and urban pollution over California: Ozone formation and air quality simulations, Atmospheric Environment, 56, 45-51, https://doi.org/10.1016/j.atmosenv.2012.03.046, 2012.

Siyan Ma, Liukang Xu, Joseph Verfaillie, Dennis Baldocchi: AmeriFlux BASE US-Var Vaira Ranch- Ione, Ver. 16-5, AmeriFlux AMP, (Dataset), https://doi.org/10.17190/AMF/1245984, 2021.

Standard operating procedures for ambient air monitoring: https://www.atmospheric-chemistry-and-physics.net/submission.html#manuscriptcomposition, May 2021.

Stavros, E. N., Abatzoglou, J. T., McKenzie, D., & Larkin, N. K.: Regional projections of the likelihood of very large wildland fires under a changing climate in the contiguous Western United States, Climatic Change, 126(3-4), 455-468, https://doi.org/10.1007/s10584-014-1229-6, 2014.

Stein, A. F., Draxler, R. R., Rolph, G. D., Stunder, B. J., Cohen, M. D., & Ngan, F.: NOAA's HYSPLIT atmospheric transport and dispersion modeling system, Bulletin of the American Meteorological Society, 96(12), 2059-2077, https://doi.org/10.1175/BAMS-D-14-00110.1, 2015.

Steinbacher, M., Zellweger, C., Schwarzenbach, B., Bugmann, S., Buchmann, B., Ordóñez, C., ... & Hueglin, C.: Nitrogen oxide measurements at rural sites in Switzerland: Bias of conventional measurement techniques, Journal of Geophysical Research: Atmospheres, 112(D11), https://doi.org/10.1029/2006JD007971, 2007.

Steiner, A. L., Davis, A. J., Sillman, S., Owen, R. C., Michalak, A. M., & Fiore, A. M.: Observed suppression of ozone formation at extremely high temperatures due to chemical and biophysical feedbacks, Proceedings of the National Academy of Sciences, 107(46), 19685-19690. https://doi.org/10.1073/pnas.1008336107, 2010.

~~Tan, Z., Lu, K., Dong, H., Hu, M., Li, X., Liu, Y., ... & Wu, Y.: Explicit diagnosis of the local ozone production rate and the ozone-NOx-VOC sensitivities, Science bulletin, 63(16), 1067-1076, https://doi.org/10.1016/j.scib.2018.01.001, 2018.~~

Trainer, M., Parrish, D. D., Buhr, M. P., Norton, R. B., Fehsenfeld, F. C., Anlauf, K. G., ... & Tanner, R. L.: Correlation of ozone with NOy in photochemically aged air, Journal of Geophysical Research: Atmospheres, 98(D2), 2917-2925, https://doi.org/10.1029/92JD01910, 1993.

Trebs, I., Bohn, B., Ammann, C., Rummel, U., Blumthaler, M., Königstedt, R., ... & Andreae, M. O.: Relationship between the NO_2 photolysis frequency and the solar global irradiance, Atmospheric Measurement Techniques, 2(2), 725-739, https://doi.org/10.5194/amt-2-725-2009, 2009.

Trousdell, J. F., Caputi, D., Smoot, J., Conley, S. A., & Faloona, I. C.: Photochemical production of ozone and emissions of NO x and CH 4 in the San Joaquin Valley. *Atmospheric Chemistry and Physics*, *19*(16), 10697-10716, https://doi.org/10.5194/acp-19-10697-2019, 2019.

Trousdell, Justin F., Stephen A. Conley, Andy Post, and Ian C. Faloona: Observing entrainment mixing, photochemical ozone production, and regional methane emissions by aircraft using a simple mixed-layer framework, Atmospheric Chemistry and Physics, 16, no. 24, 15433-15450, https://doi.org/10.5194/acp-16-15433-2016, 2016.

Val Martín, M. V., Honrath, R. E., Owen, R. C., Pfister, G., Fialho, P., & Barata, F.: Significant enhancements of nitrogen oxides, black carbon, and ozone in the North Atlantic lower free troposphere resulting from North American boreal wildfires, Journal of Geophysical Research: Atmospheres, 111(D23), https://doi.org/10.1029/2006JD007530, 2006.

Volz-Thomas, A., Pätz, H. W., Houben, N., Konrad, S., Mihelcic, D., Klüpfel, T., & Perner, D.: Inorganic trace gases and peroxy radicals during BERLIOZ at Pabstthum: An investigation of the photostationary state of NOx and O3, Journal of Geophysical Research: Atmospheres, 108(D4), PHO-4, https://doi.org/10.1029/2001JD001255, 2003.

Wendisch, M., Mertes, S., Ruggaber, A., & Nakajima, T.: Vertical profiles of aerosol and radiation and the influence of a temperature inversion: Measurements and radiative transfer calculations, Journal of Applied Meteorology, 35(10), 1703-1715, https://doi.org/10.1175/15200450(1996)035<1703:VPOAAR>2.0.CO;2, 1996.

Formatted: Pattern: Clear (White)

Xu, Z., Wang, T., Xue, L. K., Louie, P. K., Luk, C. W., Gao, J., ... & Wang, W. X.: Evaluating the uncertainties of thermal catalytic conversion in measuring atmospheric nitrogen dioxide at four differently polluted sites in China. *Atmospheric Environment*, *76*, 221-226, https://doi.org/10.1016/j.atmosenv.2012.09.043, 2013.

830

Zhang, L., Jacob, D. J., Yue, X., Downey, N. V., Wood, D. A., & Blewitt, D.: Sources contributing to background surface ozone in the US Intermountain West, Atmospheric Chemistry and Physics, https://doi.org/10.5194/acp-14-5295-2014, 2014.

Zhong, S., Whiteman, C. D., & Bian, X.: Diurnal evolution of three-dimensional wind and temperature structure in

835

California's Central Valley, Journal of Applied Meteorology, 43(11), 1679-1699, https://doi.org/10.1175/JAM2154.1, 2004.